# Development of Ultrasound-Triggered Antibiotic Release Clip to Prevent Spinal Fusion Infection

A Thesis

Submitted to the Faculty

of

Drexel University

by

Alex Michael Sevit

in partial fulfillment of the

requirements for the degree

of

Master of Science in Biomedical Engineering

June 2015

*This work would not have been possible without my lab mates and mentors at the Implant Research Center and Thomas Jefferson University. Thank you for your knowledge and support over the past four years.*

## TABLE OF CONTENTS

LIST OF TABLES ……vi

LIST OF FIGURES ……..vii

ABSTRACT…….x

1. INTRODUCTION……..…..……...…1

1.1 Lumbar Spinal Fusion Surgery……..1

1.2 Infection in Spinal Fusion Surgery……3

1.3 Biofilm Infections…….....4

1.4 Prophylactic Techniques to Combat SSI……...6

2. DEVICE DESIGN…….……9

2.1 Problem Definition……9

2.2 Design Rationale……..10

2.3 Design Overview……11

2.4 Design Criteria…….....13

2.5 Comparative Decision Matrix……..14

3. SPECIFIC AIM 1: Manufacture and Verify Clip..……...……..……17

3.1 Aim Description and Hypotheses……17

3.2 Poly(Ether Ether Ketone)…….....17

3.3 Selective Laser Sintering……18

3.4 Design and Manufacturing……...20

3.5 Porosity Analysis……...……..23

3.6 Discussion……..25

4. SPECIFIC AIM 3: Model Release Rate and Validate……...…….....26

4.1 Aim Description and Hypothesis…….26

4.2 Model Development……....26

4.3 Model Validation Release Experiment……31

4.4 Results…….…….....32

4.5 Discussion……34

5. SPECIFIC AIM 3: Membrane Development…….....39

5.1 Aim Description and Hypotheses……....39

5.2 Ultrasound-Triggered Drug Delivery……..39

5.3 Alternative Triggered Drug Delivery Techniques……...40

5.4 Poly(Lactic Acid)…….....42

5.5 Membrane Development…….43

5.6 Membrane Retention and Release Experiment……44

5.7 Results……..45

5.8 Discussion……53

6. CONCLUSION AND FUTURE WORK……...……..56

WORKS CITED……..……...62

## LIST OF TABLES

Table 1: Comparative matrix ranking three local antibiotic administration methods on key criteria. Often the ranking is tied between two approaches, thus two approaches will be granted the same score……...14

Table 2: Values input into the mathematical model to predict drug release rate from the clip……..33

Table 3: Previously-determined values of the diffusion coefficient of methylene blue…35

## LIST OF FIGURES

Figure 1: Rigid internal fixation retrieval, courtesy of the Implant Research Center (Drexel University). The titanium rod mimics the curvature of the lumbar spine and is anchored to the vertebrae via the pedicle screws, providing immediate stability to the spine....……..2

Figure 2: Proteins adsorb to and decorate the surface of an implanted device. Planktonic bacteria (green) colonize the surface and begin proliferating. Through quorum sensing, the bacteria change to the sessile phenotype (pink) and secrete a glycocalyx matrix (purple). Bacteria near the surface of the biofilm detach and revert back to their planktonic state, causing a chronic infection…….....5

Figure 3: Summary of prophylactic antimicrobial practices and their intervention within the development of a biofilm. Black points are current clinical practices and red points are surface coatings under investigation……..9

Figure 4: The device is a clip (tan) that can engage with a spinal fusion rod. (A) With the application of ultrasound, a supra-therapeutic dose of antibiotic is released directly into the wound site. (B) Ultrasound will disrupt the bacterial biofilm on the implant surface and enhance both sessile (pink) and planktonic (green) bacterial susceptibility to the antibiotic. …….....11

Figure 5: The SLS PEEK clip will attach to a spinal fusion rod at the time of surgery, initially containing a dose of antibiotic. The antibiotic is contained within a poly(lactic acid) membrane, which will rupture in response to an ultrasound trigger…….....12

Figure 6: Individual particles are distributed in a thin layer and heated to just below melting temperature. After application of the laser, molten particles fuse together to form a solid construct, however, particle fusion is often incomplete, resulting in a porous material……..19

Figure 7: (A) Tri-level spinal fusion rod retrieval has clear notches indicating where the pedicle screws interface with the rod. The distance between notches (B) was measured as 12 mm. The height of the clip was designed to allow 1.5 mm of clearance on each side so the pedicle screws do not impinge on the clip……...20

Figure 8: Clips attach to the 5.5 mm spinal fusion rod with moderate force and fit flush against the rod……21

Figure 9: (From left to right): Frontal, isometric, and top view of Solidworks drawings of the clip. Six critical dimensions were measured via μCT……22

Figure 10: Comparison of designed and measured clip dimensions of four devices reveals no significant difference……...22

Figure 11: (A) Cross-section of a μCT rendering reveals pores distributed throughout the material. (B) Histogram of pore size distribution normalized to total porous space…….23

Figure 12: SEM Images of the material surface. (top) 500 x image shows individual particles ranging from 1 to 100 μm that are only partially sintered. (bottom) 120 x image shows voids throughout the un-fused particles……..24

Figure 13: Release through the drug delivery channel is constant. Concentration within the clip is constant as drug is constantly dissolving, while outside of the clip is an infinite sink (drug concentration is 0)……...27

Figure 14: Release through the porous walls is constant. Concentration within the clip is constant as drug is constantly dissolving, while outside of the clip is an infinite sink (drug concentration is 0)……..28

Figure 15: Boundary conditions used to analytically solve Equation 2.1……..……29

Figure 16: Release results were fit to a linear regression ($R^2$=0.996), revealing a 3.27% release rate over the first 3 hours……...32

Figure 17: Release profile extended over 10 hours shows divergence from model at 3 hours……...34

Figure 18: (A) Batch one clips were dried on their tops and were difficult to remove from the bench top after drying. (B) Batch two clips were dried on their flanges, minimizing interfacial area with the bench top……44

Figure 19: Mass measurements taken before and after coating. (Top) Measurements of the batch one clips show the 5-50 clips contained 80 mg of PLA, the 10-50 clips had 161 mg and the 5-250 clips contained 173.5 mg. (Bottom) An order of magnitude less PLA was deposited on the 5-50 and 10-50 batch two clips. However, 80 mg more PLA was deposited on the surface of the 5-250 clips of batch two than batch one……..47

Figure 20: (Top) SEM image of the un-coated SLS PEEK material. (Bottom) The surface of the material coated with the 5-50 technique. PLA is deposited on the surface and within the pores, although pores are still visible…….....48

Figure 21: (Top) Surface of the 10-50 shows even more PLA deposition than the 5-50 technique, although pores are still visible through (Bottom) The 5-250 membrane is a thick layer that completely hides the original morphology of the SLS PEEK surface…..49

Figure 22: The 5-250 clips allowed for 19% MeB release over the first week, while 5-50 and 10-50 clips both allowed 38% release. Ultrasound was applied at day 7 and release was observed an additional 24 hours past……..50

Figure 23: Pre-sonication release was fastest in the 5-50 group and slowest for the 5-250 group. Post-sonication, release was accelerated in the 5-50 and 10-50 groups. Release decelerated slightly in the 5-250 group……..51

Figure 24: (top) Batch two release profiles during the first seven days of incubation. (bottom) Additional release following ultrasound triggering at the end of day……....52

Figure 25: Defect observed on the surface of the 5-250 clip was probably the result of handling during and directly after coating…….....54

Figure 26: Possible second iteration of the clip, featuring more drug delivery channels and a smaller clip wall. According to the model, this clip would release drug faster than the previous clip version……58

Figure 27: The PEEK clip will act as a tertiary defense system within the scope of standard clinical infection prophylaxis. It could also work in synergy with passive antimicrobial coatings currently under investigation..……60

## ABSTRACT

Surgical site infection (SSI) is a devastating outcome of lumbar fusion surgery arising in 8.5% of primary procedures. This infection is often marked by the formation of biofilm, which is highly resistant to antibiotics, thus the only treatment for SSI is secondary surgery. Ultrasound has been recently found to mechanically disrupt biofilm, increasing its antibiotic susceptibility, and is often used to trigger drug release. In this study, an ultrasound-triggered antibiotic release device has been developed. The device is made of selective laser sintered polyetheretherketone (PEEK) and clips to a standard 5.5 mm lumbar fusion rod. Initially, the clip will be loaded with antibiotic and sealed with a poly(lactic acid) (PLA) membrane, however, with application of ultrasound, the membrane will rupture, releasing antibiotic directly into the surgical site. Dimensional accuracy was verified using computer tomography and the SLS PEEK material was found to be 38% porous. A model was developed to understand the mechanism of release from the clip. The model supported the hypothesis that release occurred through the walls of the clip as well as from the drug delivery channel, highlighting the necessity of a robust membrane to retain drug. The membrane was applied via submersion in a PLA-chloroform solution. The amount of PLA deposited on the clip was varied by changing the number of dips and the concentration of PLA. To assess membrane drug retention and responsiveness to ultrasound-triggered release, clips were incubated for 7 days in physiological conditions, then sonicated at day 7. The high concentration membrane showed the greatest retention, retaining 81% of the loaded drug over 7 days, however, it was unperturbed by ultrasound. The low concentration clips only retained 62% of their drug, but showed an increase in release rate after ultrasound. Further investigation should

focus on membrane optimization: finding the precise number of dips and PLA concentration to fulfill the design criteria. The next step would then be to assess the antibacterial effectiveness of the device. This study has demonstrated promising initial feasibility of the drug delivery clip. With further development, this device could be implemented with current clinical antibiotic prophylaxis, to provide another layer of protection. This staged treatment with antibiotics could further reduce the incidence of surgical site infection, decreasing health care costs, disability of this serious complication.

# 1. INTRODUCTION

## *1.1 Lumbar Spinal Fusion Surgery*

Lumbar posterior fusion surgery (LPFS) is a procedure used to restore mechanical stability to the lumbar region of the spine [1]. While the technique and instrumentation have changed since the procedure was first described by Albee and Hibb in 1911, the primary goal of the surgery has remained constant: to achieve bony fusion of the vertebral discs [2]. It is considered the gold standard in the treatment of congenital scoliosis and spinal collapse following tumor resection, infection, or trauma [1]. However, these indications account for only 25% of LPFS procedures performed in the United States [3]. The other 75% of procedures are prompted by intractable pain due to degenerative changes in the spine, such as disc herniation, stenosis, and disc migration [3, 4]. Despite debate in the field over the effectiveness of LPFS in treating these degenerative conditions, the rate of LPFS increased 220% between 1990 and 2005 [5, 6]. The average cost of a single procedure is $34,000, and in 2008, the total bill for all spinal surgeries performed in the United States was $33.9 billion [6].

The most common approach to LPFS is postereolateral fusion (also known as bilateral-lateral fusion, lateral mass fusion, and transverse process fusion), in which, an incision is made down the midline of the spinal column [1]. The degenerated intervertebral disc is then dissected and the space is filled with either autologous bone from the patient's iliac crest, a synthetic bone matrix, or an inter-body fusion device [1]. Regardless of type,

these fillers are meant to promote osseoinduction of the neighboring vertebrae leading to fusion and long-term stability [1].

As bony fusion takes many months to achieve mechanical stability, rigid internal fixation has been implemented to provide perioperative stability to the joint. Pedicle screws are anchored into vertebral disks and titanium rods that mimic the curvature of the spine are threaded through the screws, stabilizing them (Figure 1) [2].


Figure 1: Rigid internal fixation device, retrieval courtesy of the Implant Research Center (Drexel University). The titanium rod mimics the curvature of the lumbar spine and is anchored to the vertebrae via the pedicle screws, providing immediate stability to the spine.

While there are concerns that the rigid fixation devices induce stress shielding, thereby limiting vertebral fusion, studies have shown an 86% fusion rate in rigid fixation versus 64% fusion rate without [1].

### *1.2 Infection in Spinal Fusion Surgery*

Surgical Site Infection (SSI) arises in 8.5% of primary and 12.2 % of revision LPFS procedures according to a 2011 retrospective analysis of Medicare data [7]. Clinical presentation usually involves purulent drainage from the wound site, fever, and localized redness and tenderness [8]. Diagnosis may be confirmed by collecting a local culture and analyzing blood for increased levels of neutrophils and C-reactive proteins [9]. Gram positive bacteria, such as *S. aureus* and *S. epidermidis*, are most commonly implicated in SSI in LPFS [10]. However, gram negative bacteria, such as *E. coli* and *Enterococcus*, are also seen in 30% of SSI cases [10].

Treatment needs to be administered promptly after diagnosis, and must balance the need to maintain spinal stability with the necessity to resolve the infection [11]. A large dose of systemic antibiotics is the first step and aggressive surgical wound debridement is performed to clean the wound of bacteria [12]. In extreme cases, hardware replacement is indicated if the instrumentation is completely fouled with bacteria [12]. The average cost of treating SSI is between $15,800 and $43,900, essentially doubling the cost of the initial LPFS procedure and extending patient hospitalization and suffering [10].

Moreover, patients with major perioperative device complications (including SSI) report higher rates of pain and continued long-term disability [13].

### *1.3 Biofilm Infections*

SSI is often marked by the formation of bacterial biofilm, which ensures that bacteria are recalcitrant to antibiotic treatment and are able to subvert immune surveillance, allowing establishment of persistent infections. While the development of biofilm consists of hundreds of complex steps, there is general agreement that progression can be summarized in four major steps. Stage 1 of development is abiotic. Immediately upon implantation, the device surface is decorated with adsorbed water, albumin, lipids, and extracellular matrix (ECM) proteins [14]. This coated surface is ideal for adherence of bacterial contaminants (mostly from the air of the operating room), reversibly binding via intermolecular interactions in stage 2 of biofilm development [15]. Within hours stage 3 occurs, where these bacteria proliferate and begin producing a hydrated matrix of glycoproteins, called the glycocalax [16]. The basal layer of bacteria irreversibly bind using adhesion proteins, anchoring the biofim to the implant surface [14]. When the biofilm reaches its final stage of maturity, cells on the outer surface break off, reverting back to their planktonic phenotype [15]. These cells can circulate to other sites within the host, causing a chronic and systemic infection [17]. The stages of biofilm development are illustrated in figure 2.

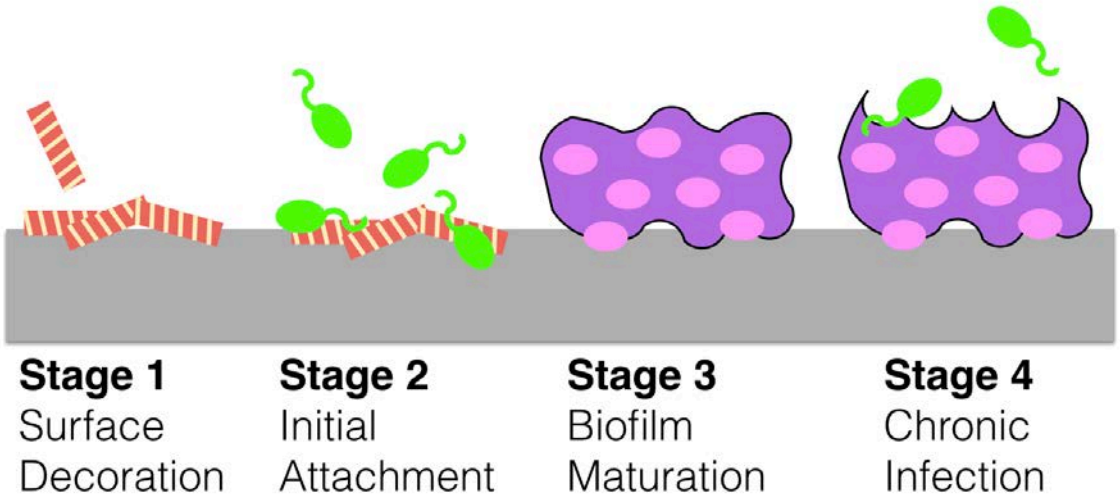


Figure 2: Proteins adsorb to and decorate the surface of an implanted device. Planktonic bacteria (green) colonize the surface and begin proliferating. Through quorum sensing, the bacteria change to the sessile phenotype (pink) and secrete a glycocalyx matrix (purple). Bacteria near the surface of the biofilm detach and revert back to their planktonic state, causing a chronic infection.

Bacteria within the biofilm develop a multi-modal tolerance to antimicrobial agents. Cells deep within the biofilm are insulated from the external environment by layers of glycocalyx, hindering antimicrobial penetration [18]. Moreover, bacteria within the matrix change phenotype, from a planktonic state to a sessile state [15]. This is due to a change in gene expression induced through intercellular quorum sensing [19]. In their sessile state, bacterial metabolism and proliferation slows; and expression of genes related to multidrug resistance increases [20]. In combination, these conditions make biofilms extremely recalcitrant to antimicrobial therapy. While the minimum inhibitory concentration of vancomycin (VAN) for planktonic *S. aureus* is 2 μg/mL, the minimum biofilm eradication concentration is reported to be 64-512 times higher [21, 22, 23].

### *1.4 Prophylactic Techniques to Combat SSI*

Due to the persistence and devastation of bacterial biofilm, the primary goal in combatting SSI in LPFS is prophylaxis. Before and after surgery, systemic antibiotics such as ampicillin are administered [24]. Advanced sterile surgical techniques are employed to minimize bacterial exposure in the operating room. This includes the use of autoclaved surgical instruments, sterile draping, and the maintenance of a sterile field of operation [9]. At the end of the implantation procedure, the wound is often packed with up to one gram of powdered vancomycin, which is meant to kill any bacteria which have entered the wound during surgery [25]. This has shown promising results: in one clinical retrospective study of 1,512 patients only 0.99% presented with infection during the 5 year study period [26]. Vacuum assisted wound closure may also be applied for one to two days post-surgery to drain edematous fluid and increase blood flow to the local region [27, 28]. While these suture drains are generally accepted in the field as beneficial for wound healing and the formation of new granulation tissue, they may conflict with antibiotic wound packing since much of the VAN packed in the wound site may evacuate through the drains, attenuating antimicrobial potential. Despite this aggressive antibiotic prophylaxis, SSI in LPFS continues to persist.

Current anti-infection biomaterials research can be broadly separated into two categories: passive surface layers that inhibit initial bacterial colonization and active surface layers that release an antimicrobial agent [29]. Silver is a popular passive surface layer that can be applied efficiently and homogeneously via ion surface deposition [30]. Silver prevents

a broad spectrum of bacteria from proliferating on an implant surface and can be functionalized with antibacterial peptides such as polymyxin B to further increase biofilm inhibition [31]. Another passive layer approach is to covalently attach poly(sulfobetaine methacrylate), creating a zwitterionic surface that inhibits protein adsorption and bacterial adhesion [32]. The primary benefit of these passive coatings is that they are generally stable and permanent, inhibiting bacterial attachment long after the perioperative period. They also do not come with a high risk of antibacterial resistance. However, they can be scratched or damaged during implantation, diminishing their effectiveness.

A common active coating is isopentyl nitrite, which releases nitric oxide, an effective bactericidal agent. In a 2015 study, inhibition of *S. epidermidis* growth was achieved over a 14 hour period using this approach [33]. Cationic antimicrobial steroid 13 was also mixed into a PDMS coating and deposited on the surface of a stainless steel plate, showing biofilm inhibition of *P. aeruginosa* over a 24 hour period [34]. Finally, PLGA microbubbles loaded with triclosan and deposited on titanium surfaces have shown degradation-controlled release over 80 hours [35]. While these coatings have all shown excellent antibacterial effect, they are limited in that their release cannot be temporally-controlled. Antibiotic release begins at implantation and is depleted within, at most, one week of the surgery. While the perioperative period is the most critical time for antimicrobial therapy, long-term infection mitigation cannot be achieved using these approaches.

### *1.5 Ultrasound-Disruption of Bacterial Biofilm*

In light of bacterial biofilm recalcitrance to antibiotic therapies, many techniques are currently under investigation to disrupt biofilms and enhance their susceptibility to antibiotics. Recently, it has been shown that low-intensity ultrasound is disruptive to biofilms and enhances both sessile and planktonic bacterial antibiotic susceptibility. One *in vitro* study showed that by treating *S. epidermitis* biofilm with VAN (100 μg/mL) and US, a significant increase in bacterial death could be achieved relative to antibiotic treatment alone [36]. The treatment was further enhanced by the addition of microbubbles, which burst in response to ultrasound, mechanically altering the biofilm surface [36]. These results have been confirmed in vitro and a similar effect has been observed on implanted polyethylene disks and antibiotic eluting bone cement in rabbits *in vivo* [36, 37, 38]. More promising still, one study has shown an increase in human neutrophil bactericidal activity stimulated by ultrasound [39]. This study demonstrated enhanced neutrophil infiltration into a fibrin gel challenged with *S. epidermidis*, mediated by surface integrin CD18 [39]. While a somewhat new approach to the treatment of biofilm infections, ultrasound has demonstrated promising enhancement to biofilm antibiotic susceptibility.

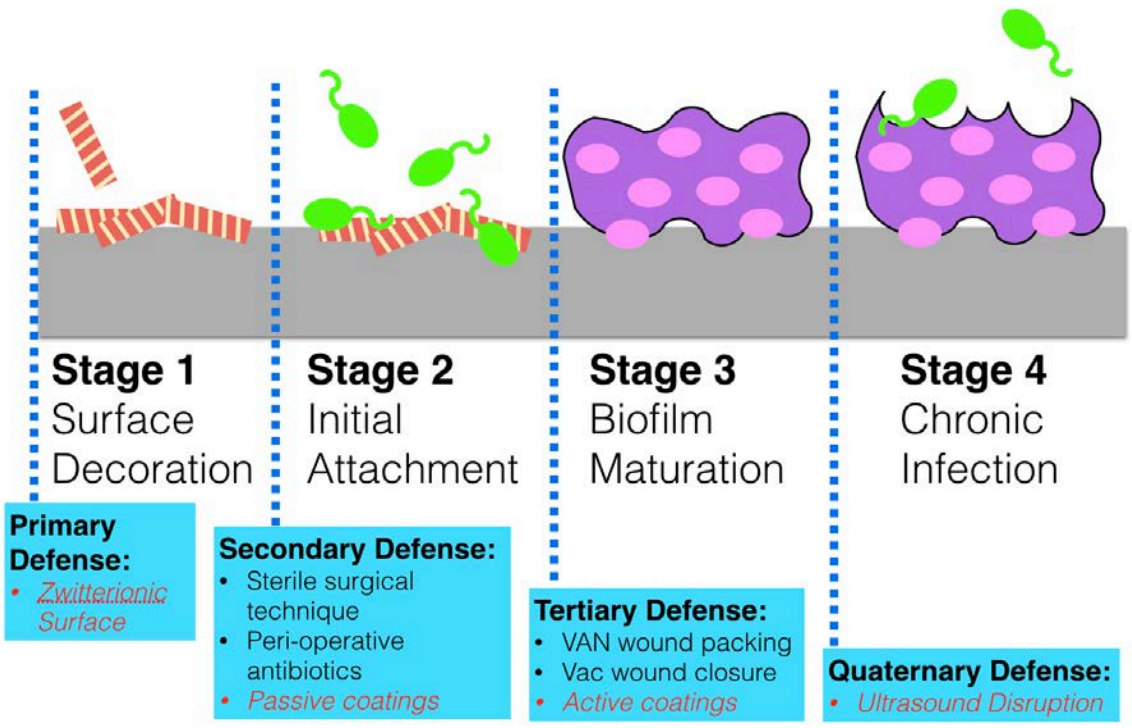


Figure 3: Summary of prophylactic antimicrobial practices and their intervention within the development of a biofilm. Black points are current clinical practices and red points are surface coatings under investigation.

## 2. DEVICE DESIGN

### *2.1 Problem Definition*

Surgical Site Infection (SSI) is a devastating outcome of lumbar spinal fusion surgery (LPFS), arising in 8.5% of primary and 12% of revision procedures [7]. SSI is often the result of biofilm formation on the implant surface, in which the bacteria create a protective gelatinous matrix of proteoglycans [16]. In this state, bacteria are extremely difficult to eradicate with systemic antibiotics and treatment is limited to secondary surgery—either aggressive debridement and irrigation of the wound or removal of current

device in extreme cases [12]. This secondary surgery prolongs patient suffering, extends hospital stay, increases mortality and can easily double the cost of the original LPFS procedure [10].

### *2.2 Design Rationale*

The goal in treating SSI must be prophylaxis. By preventing bacteria from developing into a biofilm, infection and the associated secondary surgery may be avoided. There is currently a multi-stage regimen of clinical practices aimed at preventing bacterial attachment and biofilm maturation (Figure 3). Despite these clinical practices, the incidence of infection persists so that there is an urgent need to develop further antimicrobial technology. Current biomaterials research is focused on surface coatings that prevent bacterial attachment, but no research is focused on eradicating bacteria that persist despite these defenses and begin forming biofilm. Such a contingency would add one more barrier for bacteria to overcome in the development of a biofilm and thus would reduce incidence of SSI. In this study we will develop a drug-filled clip for ultrasound-triggered release of antibiotics to the LPFS surgical site one week after implantation. Not only will a supra-therapeutic dose of antibiotic be delivered to the surgical site, but ultrasound has been shown to enhance biofilm antibiotic susceptibility (Figure 4). This two-pronged attack should eradicate any remaining bacteria in the surgical site that would have the potential to develop into surgical site infection.

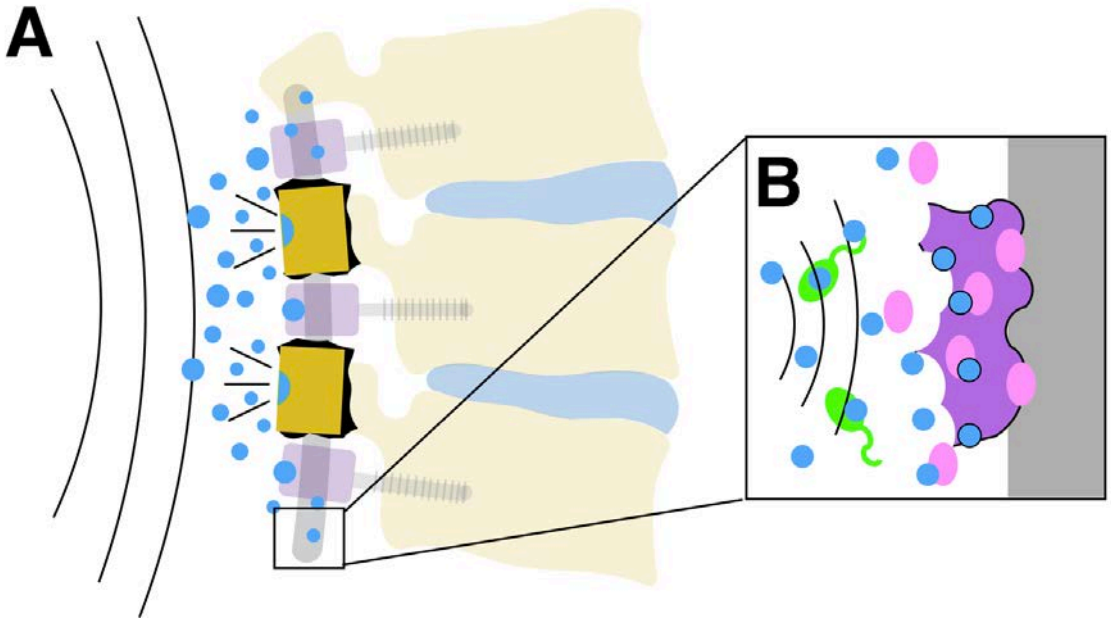


Figure 4: The device is a clip (tan) that can engage with a spinal fusion rod. (A) With the application of ultrasound, a supra-therapeutic dose of antibiotic is released directly into the wound site. (B) Ultrasound will disrupt the bacterial biofilm on the implant surface and enhance both sessile (pink) and planktonic (green) bacterial susceptibility to the antibiotic.

### *2.3 Design Overview*

The device is a clip, manufactured in selective laser sintered (SLS) polyetheretherketone (PEEK) that attaches to a standard 5.5 mm lumbar spinal fusion rod. The clip houses a reservoir containing a dose of powdered antibiotic. While the precise dose will ultimately depend on the density of selected antibiotic, we have found the clip can hold 120 mg of methylene blue, which is a dye whose solubility and density are similar to vancomycin, a widely-used antibiotic. A key strength of this device is that multiple antibiotics can be loaded into the reservoir to eradicate a broad range of bacterial species. The drug will be sealed within the clip by a hydrophobic poly(lactic acid) membrane.

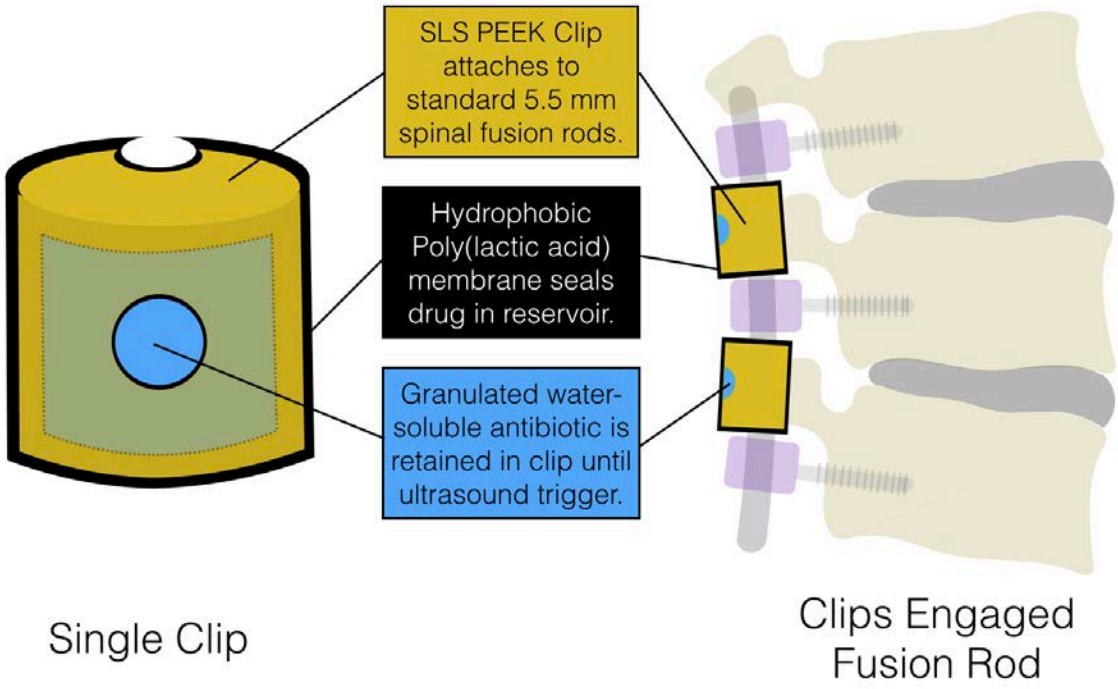


Figure 5: The SLS PEEK clip will attach to a spinal fusion rod at the time of surgery, initially containing a dose of antibiotic. The antibiotic is contained within a poly(lactic acid) membrane, which will rupture in response to an ultrasound trigger.

The device will be initially clipped onto the spinal fusion rod at the time of surgery. During the first week following implantation, the clip will remain inactive in the wound site, simply retaining the antibiotic. Approximately one week post-implantation, ultrasound will be applied to the wound site, which will rupture the PLA membrane and release antibiotic into the surgical site.

## *2.4 Design Criteria*

1. **Clip to a standard 5.5 mm spinal fusion rod without impeding the primary function of the device.**

   The primary function of a spinal fusion rod is to stabilize the spinal column and promote boney fusion between vertebrae. Pedicle screws, attached to the rod, are drilled into the vertebral disks, anchoring them in place. The clip will attach to the rod in between pedicle screws. Careful consideration must be made when designing the device so that the clip does not impinge on the pedicle screws. Moreover, the clip interface must be dimensioned so that it fits flush against the spinal fusion rod.

2. **Retain drug in reservoir for 1 week without leakage.**

   The membrane must retain drug at least as long as vacuum suture drains are implanted, which is typically two to three days. Ideally, the drug would be released right after removal of suture drains when there is the minimum amount of bacteria in the wound space. The one-week range was chosen to demonstrate the range of flexibility a clinician would have in triggering release. Minimizing leakage is important because there would be less antibiotic to deliver during triggered release, attenuating the efficacy of the treatment.

3. **Trigger release of drug with ultrasound, achieving complete release within 24 hours.**

The goal of the antibiotic therapy is to deliver a supratherapeutic surge of antibiotic directly to the wound site to kill all bacteria. Therefore, the goal is a triggered quick and complete release. Incomplete release may result in extended subtherepeutic levels of antibiotic, which may give rise to antibiotic resistant bacteria.

### *2.5 Comparative Decision Matrix*

Three local antibiotic delivery methods were compared on multiple criteria. Numbers in the matrix represent a ranking: 1 is the worst ranking while 3 is the best. Active drug release coatings are currently under investigation to deliver antibiotics directly to the surgical site during the peri-operative period. Surgical site injection is an injection of antibiotic directly to the wound site following removal of suture drains.

Table 1: Comparative matrix ranking three local antibiotic administration methods on key criteria. Often the ranking is tied between two approaches, thus two approaches will be granted the same score.

| Criteria | PEEK Clip | Active Coating | Surgical Site Injection |
|---|---|---|---|
| 1. Least invasive | 2 | 2 | 1 |
| 2. Min. loss from drains | 2 | 1 | 2 |
| 3. Min. human error | 2 | 2 | 1 |
| 4. Min. surgical damage | 2 | 1 | 2 |
| 5. Synergy with other tech | 3 | 1 | 2 |
| 6. Min. long term effects | 1 | 2 | 2 |
| 7. Enhanced by US | 3 | 1 | 1 |
| **Total** | **15** | **10** | **11** |

1. The SLS PEEK Clip and active coating are both equally invasive as they are both implemented in a minor step during implantation surgery. Injection is more invasive since it will introduce a foreign object with the potential for skin contamination and cause tissue disruption to an already painful surgical site.
2. Because the clip and the injection would both administer antibiotic after removal of vacuum suture drains, they both equally minimize antibiotic loss. Active coatings lack temporal control, thus release will begin at the time of surgery and antibiotic will be lost to suture drains attenuating antibiotic therapy.
3. Surgical site injection has the largest propensity for human error since an injection to one area of the surgical site will not ensure coverage over the entire device. In fact, there would be no way of knowing if the antibiotic even made it to the implant where it would be most effective at eradicating adherent bacteria. The clip and the antibiotic coating both require minimal implementation on the part of the surgeon and both have a low propensity for human error.
4. A major disadvantage of any antibiotic coating is that it may be damaged during surgery through scratching or shearing. The clip is attached after instrumentation has been implanted, thus it is unlikely that it would sustain any surgical damage that would impair its function. Injection would occur long after surgery so it has no potential for surgical damage.
5. The biggest advantage of the clip is that it will work in synergy with other antibiotic prophylaxis. The clip could be used in synergy with a passive antimicrobial coating, delivering antibiotic peri-operatively, while the coating

could remain to prevent attachment of bacteria long-term. An active coating displaces the potential for any long-term passive coating. Once it releases its drug, it is essentially useless.

6. An undeniable disadvantage of the clip is that, after release of antibiotic, it remains attached to the implant. Active coatings do as well, however, they do not add as much bulk to an instrumented spinal fusion system as the clip. Moreover, injection does not entail any implantation, thus, there would be no long-term effects from an injection.
7. Recent revelations about biofilm-disrupting effects of ultrasound have shown great clinical promise. However, there is currently no method for delivering antibiotics to the surgical site in tandem with biofilm. The antibiotic released from the clip would have an enhanced effect on biofilm because of the administration of ultrasound, making this therapy superior to active release coatings and surgical site injections.

# 3. SPECIFIC AIM 1: Manufacture and Verify Clip

## *3.1 Aim Description and Hypothesis*

The clip will be manufactured in selective laser sintered poly(ether ether ketone) (SLS PEEK). This manufacturing process takes an input CAD file and builds a solid part, layer by layer, that is (in theory) an exact replica of the input file. To ensure the clip is accurately manufactured, critical dimensions of the clip will be measured using micro computer cosmography (μCT). SLS is known for producing porous materials. Because this could potentially present another path of escape for drug within the reservoir, porosity will also be assessed using μCT. The two hypotheses of this aim are:

1. There will be no significant difference between the dimensions of the CAD drawing and the dimensions of the SLS PEEK clip.
2. The SLS PEEK Material will be porous.

## *3.2 Polyetheretherketone (PEEK)*

PEEK is a hydrophobic polymer with a precedent of success in the spine. PEEK spinal fusion rods are gaining popularity as semi-rigid instrumentation, which allow for a greater range of motion and better stress distribution than stainless steel rods [40]. Anterior lumbar fusion cages made of PEEK have also been used to promote fusion while restoring disc height and providing perioperative stability [41]. There are a few key

properties that make PEEK an excellent material for implantable medical devices. With a glass transition temperature of 143 ºC, the polymer behaves like a crystalline solid at body temperature, conferring an elastic modulus between 3 and 4 GPa [42]. Its melting temperature is 343ºC, meaning PEEK can be autoclaved repeatedly with virtually no effect on the surface or bulk properties [42]. It is also chemically stable, and does not succumb to conventional modes of polymer degradation such as hydrolysis [43].

### *3.3 Selective Laser Sintering*

Currently the only clinical use of PEEK implants manufactured via Selective Laser Sintering (SLS) is in treating craniofacial defects [44]. SLS PEEK is optimal for this application because patient-specific cranial implants can be rapidly manufactured within a matter of days. Three dimensional computer-aided design (CAD) files are input into the SLS machine to specify the dimensions and shape of the part [45]. A thin layer of PEEK powder, 100-200 μm thick, is spread across a plate and heated to just below the polymer melting point. Orchestrated by the beam deflection system, a laser is applied to the powder, melting the PEEK and allowing them to flow together. After cooling, a single solid cross section of the part is generated while particles on the plate that have not been sintered remain as loose powder. Then another thin layer of powder is spread and the process repeats, creating a 3-dimensional construct that is an agglomeration of many layers of melted and re-solidified polymer.

Like many other additive manufacturing techniques such as 3-dimensional printing, there is an inherent porosity to the material. In the case of SLS, this is due to incomplete particle fusion, where the particles in their molten state do not completely fuse together to form a solid construct (Figure 6).

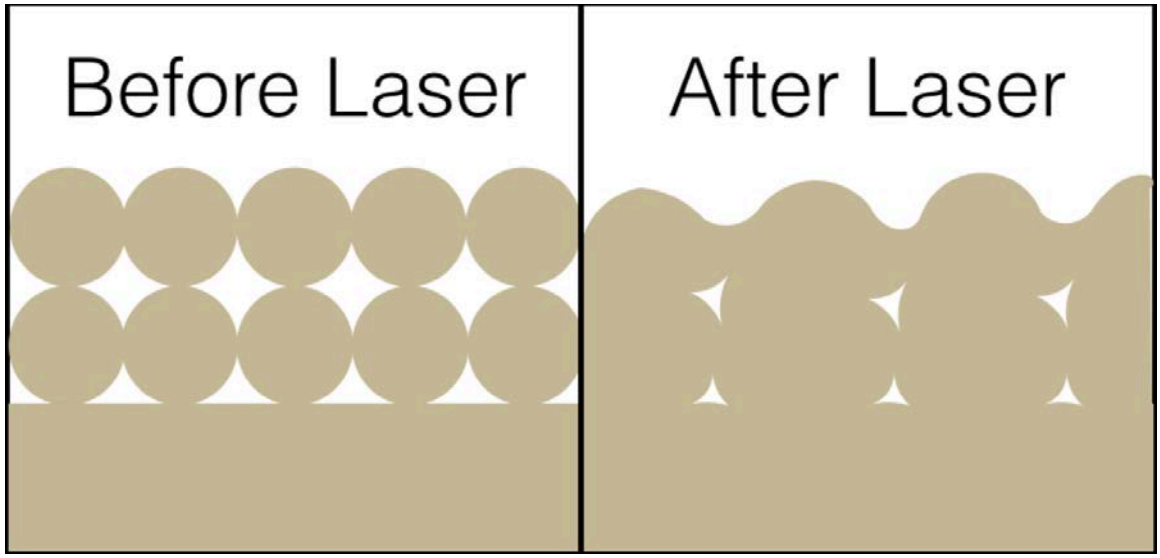


Figure 6: Individual particles are distributed in a thin layer and heated to just below melting temperature. After application of the laser, molten particles fuse together to form a solid construct, however, particle fusion is often incomplete, resulting in a porous material.

SLS manufacturing parameters can be altered to minimize material porosity. For instance, particle morphology plays a large role in material porosity. Irregularly shaped particles with sharp angles and "flaky" edges will not flow together as well during sintering, leading to more porosity [46]. Porosity is also inversely proportional to laser energy density, indicating that more particle flow is achieved when more energy is applied [47].

### *3.4 Design and Manufacturing*

To design a clip that properly attaches to a standard 5.5 mm spinal fusion rod and does not impinge on pedicle screw placement, key dimensions were measured from a tri-level spinal fusion rod retrieval (courtesy of the Implant Research Center, Drexel University, Philadelphia, PA). Because the pedicle screws interface very tightly with the fusion rod, marks can be observed on the surface (figure 7).


Figure 7: (A) Tri-level spinal fusion rod retrieval has clear notches indicating where the pedicle screws interface with the rod. The distance between notches (B) was measured as 12 mm. The height of the clip was designed to allow 1.5 mm of clearance on each side so the pedicle screws do not impinge on the clip.

The distance between these marks was 12.00 mm, which was taken as the amount of room on the rod for the clip. The final clip height was 3 mm shorter than this distance to allow plenty of space between the pedicle screws and the clip. The clip was designed in Solidworks 2014. STereoLithography (.STL) files were sent to the Centre for Additive Layer Manufacturing at University of Exeter (Exeter, UK) and manufactured in SLS PEEK. Upon receipt from Exeter University, clipping action was qualitatively assessed using a standard 5.5 mm spinal fusion rod retrieval (Figure 8).

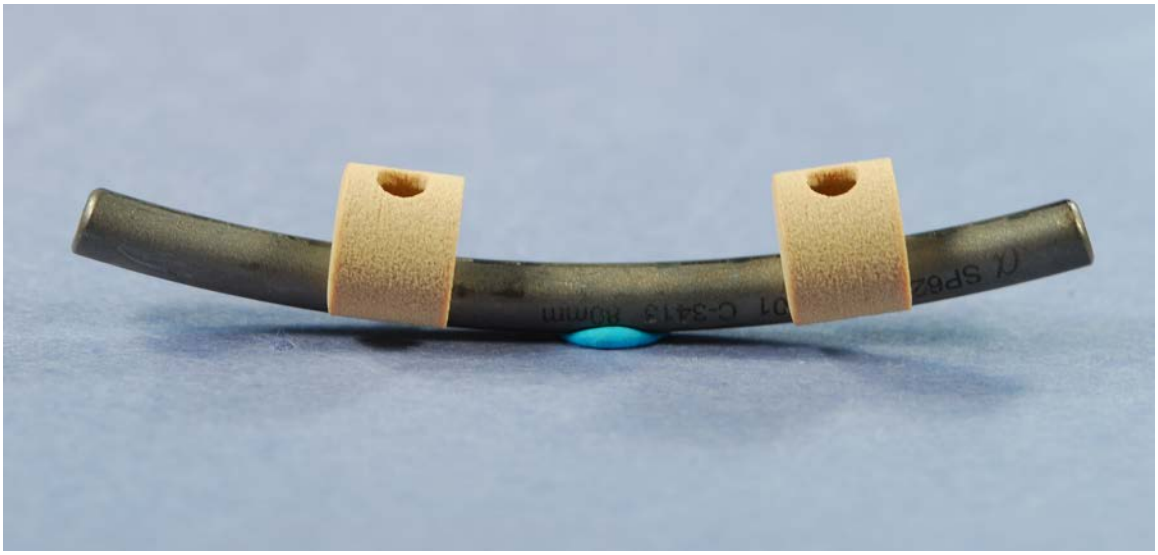

Figure 8: Clips attach to the 5.5 mm spinal fusion rod with moderate force and fit flush against the rod.

The clipping test revealed that moderate force was required to attach the device to the rod. Once attached, the clip fits flush against the rod and does not slide down the rod. Accuracy of six critical dimensions on four clips was assessed via Scanco μCT 80 (0.01

voxel resolution). They were the width and height of the cylindrical clip, the thickness of the wall, the horizontal and vertical diameters of the drug delivery channel, and the diameter of the clip interface (Figure 9). Four clips were scanned and measured to ensure repeatability of manufacturing. Measurements revealed no significant difference between any of the measured and designed dimensions when compared via a student's t-test ($\alpha<0.05$).

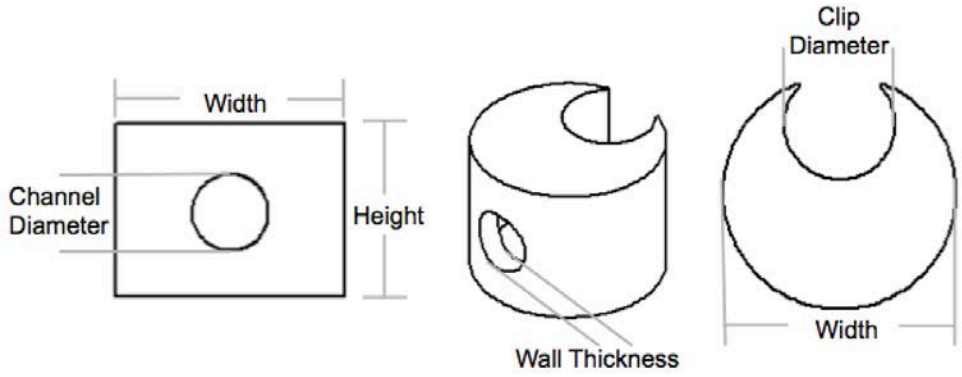


Figure 9 (From left to right): Frontal, isometric, and top view of Solidworks drawings of the clip. Six critical dimensions were measured via μCT.

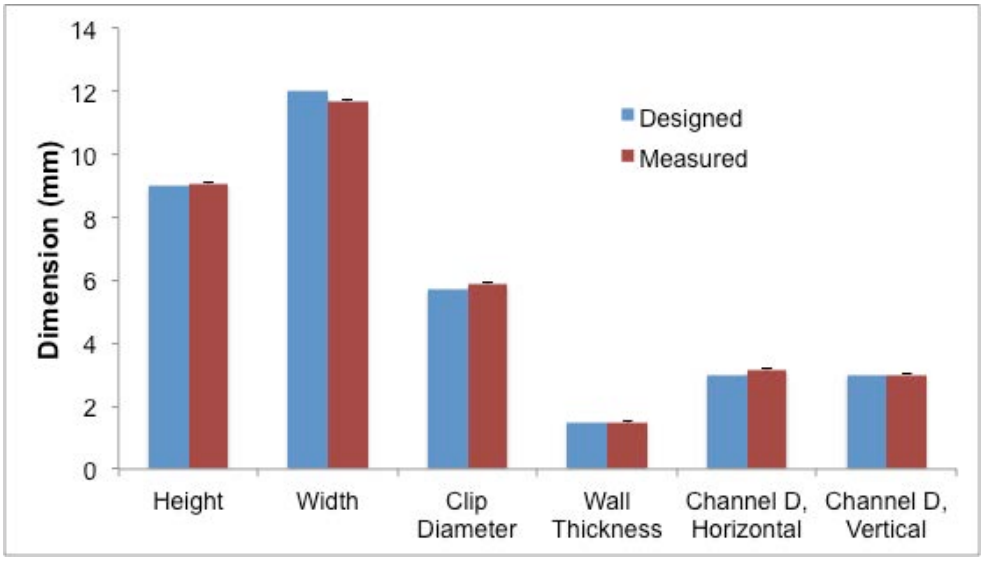


Figure 10: Comparison of designed and measured clip dimensions of four devices reveals no significant difference.

### *3.5 Porosity Analysis*

One clip underwent μCT porosity analysis, which revealed 38% porosity and an average pore size of 0.23 mm.

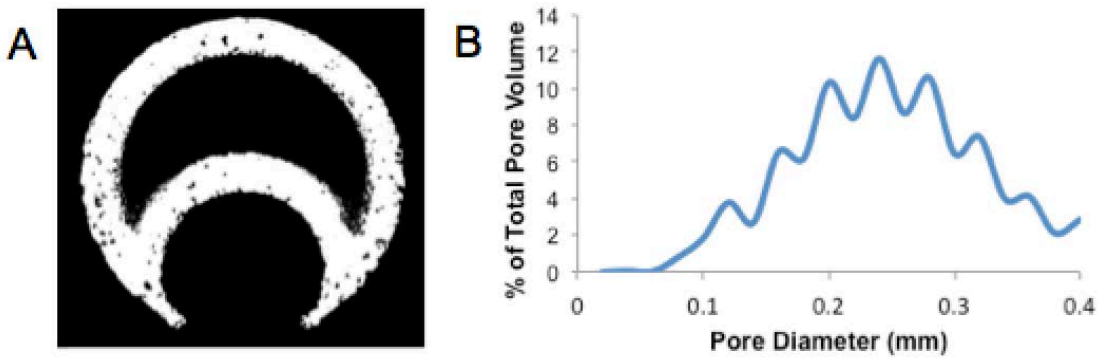


Figure 11: (A) Cross-section of a μCT rendering reveals pores distributed throughout the material. (B) Histogram of pore size distribution normalized to total porous space.

The clips were also imaged using scanning electron microscopy (SEM) with an electron beam voltage of 5 kV at a working distance of 18.44 mm. Prior to imaging the surface was sputter coated with platinum (40 mA current, 40 seconds). The high magnification image (500 x) shows sintered PEEK particles on the surface of the clip ranging from 1 μm to 100 μm. The low magnification image (120 x) illustrates the bulk appearance of the material. Large voids were observed between the particles, supporting the findings of the μCT study.

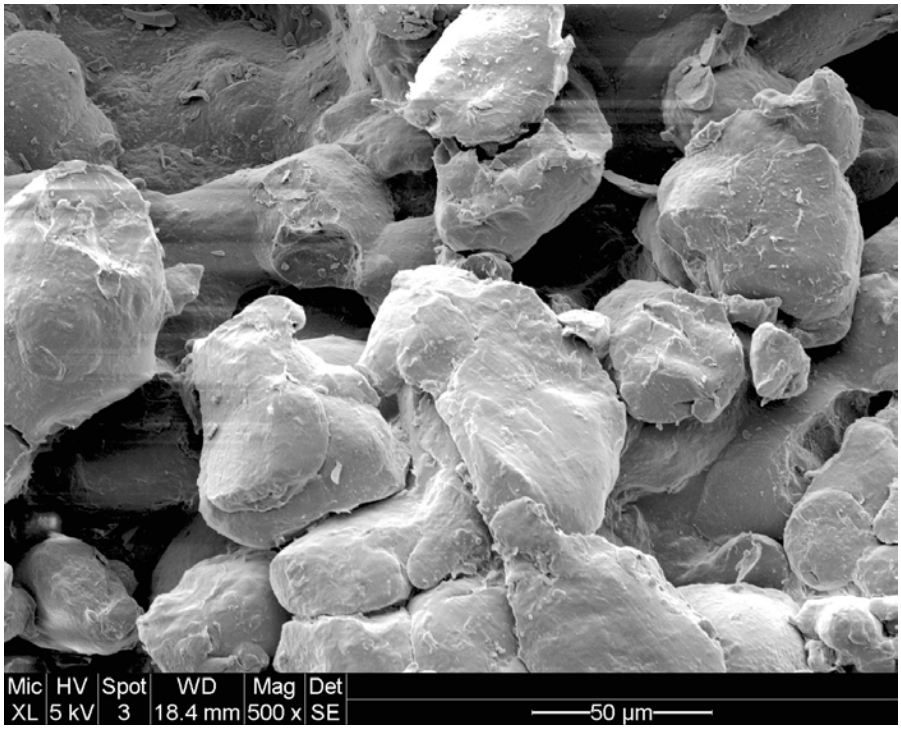


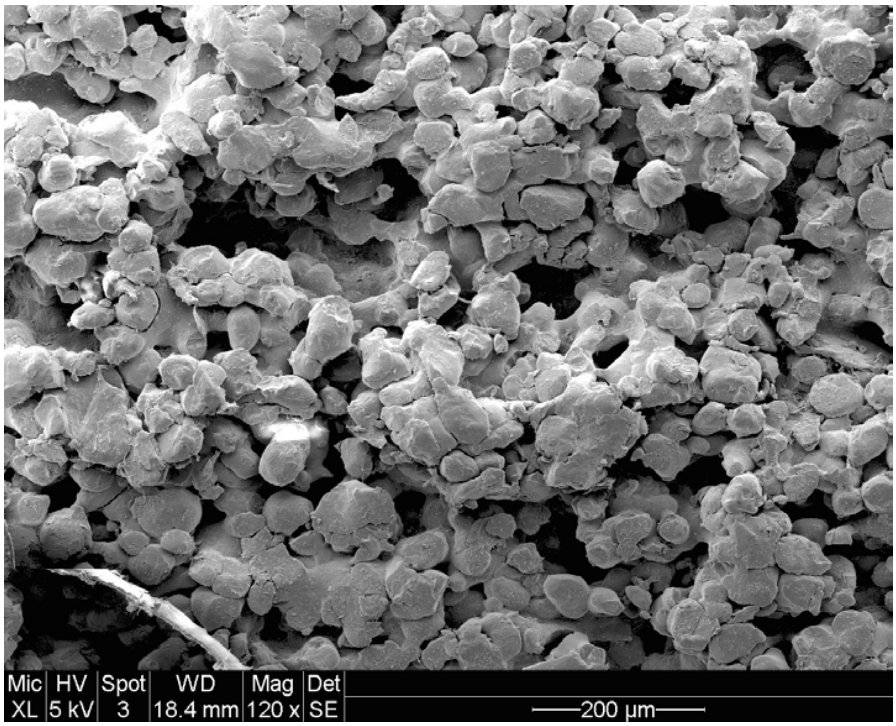


Figure 12: SEM Images of the material surface. (top) 500 x image shows individual particles ranging from 1 to 100 µm that are only partially sintered. (bottom) 120 x image shows voids throughout the un-fused particles.

### *3.6 Discussion*

This assessment demonstrated that SLS was an effective technique for manufacturing the drug delivery clip. Hypothesis 1 was supported, in that there were no significant differences between the Solidworks design and the physical clip (Figure 10). This analysis was performed on four clips demonstrating that the manufacturing technique was repeatable. The clip also fits flush against a spinal fusion rod retrieval, showing resistance to longitudinal sliding. Although not quantitatively assessed, the clip attached to the spinal fusion rod retrieval with moderate force. Ease of clipping gives the rod good clinical translatability as the device will not prolong procedure time. Moreover, surgeons will have to undergo minimal training to use this device.

As is the case for all materials made through additive manufacturing techniques, SLS PEEK is inherently porous, supporting hypothesis 2. This is primarily due to incomplete particle fusion in which the particles do not completely flow together during laser sintering, seen in the SEM images (figure 12). As seen in the cross section of figure 11, pores are homogenously dispersed throughout the material and are an average size of 0.23 mm. The SEM images further illustrate the incomplete particle fusion, as individual PEEK particles are clearly visible on the material surface. It is almost certain that release will proceed through the voids between these un-fused particles, therefore, this release will have to be taken into account during model development in aim 2.

# 4. SPECIFIC AIM 2: Model Release Rate and Validate

## *4.1 Aim Description and Hypothesis*

Before applying a membrane, it is important to determine how fast drug will release from an uncoated clip. The addition of a membrane will slow release, therefore, the rate determined here will be the fastest possible. Since the clip was found to be 38% porous in aim 1, it is also important to assess any leakage out of the porous walls. If leakage does occur from the walls, it will motivate the application of a membrane around the entire clip instead of simply sealing the drug delivery channel. The hypothesis of this aim is:

1. Release from the clip can be accurately modeled using a steady state dissolution-diffusion model.

## *4.2 Model Development*

The model developed uses Noyes-Whitney principles to consider the dissolution of solid drug and Fick's laws to consider diffusion out of the device. Two modes of drug release are analyzed: out of the drug-delivery channel and out of the porous walls of the SLS PEEK material.

### *4.2.1 Release from Drug Delivery Channel*

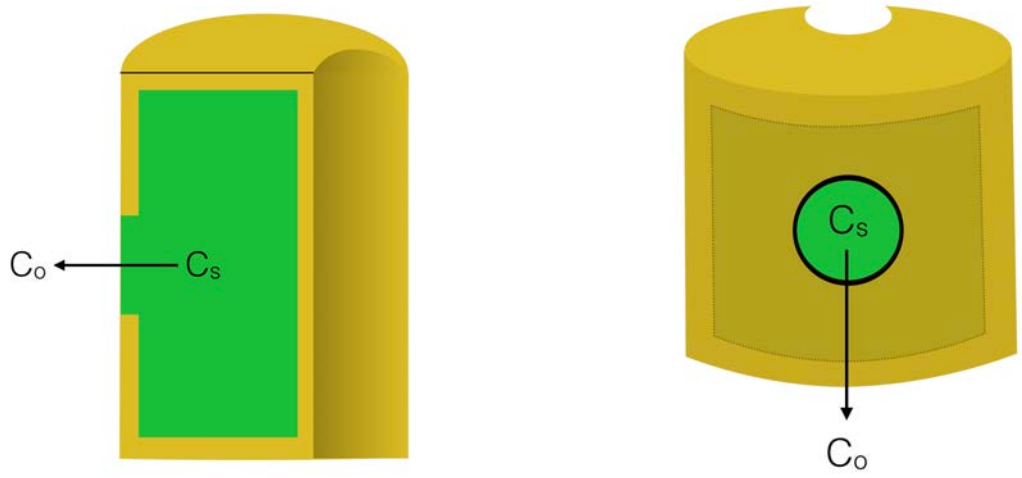


Figure 13: Release through the drug delivery channel is constant. Concentration within the clip is constant as drug is constantly dissolving, while outside of the clip is an infinite sink (drug concentration is 0).

When drug releases through the delivery channel, it diffuses down a linear concentration gradient according to Fick's law of diffusion.

$$N = D\frac{\partial c}{\partial x} \quad \text{(equation 1.1)}$$

Where N is the molar flux and D is the diffusion coefficient. Because drug is constantly dissolving within the reservoir, we consider the concentration (c) of drug within the reservoir constant and equal to the solubility of methylene blue, $C_S$. We also consider the media around the clip to be an infinite sink in which the concentration of drug is zero. This is because *in vivo*, the antibiotic will quickly be swept away from the clip by the vascular system. Finally, the distance between the source and sink is equal to the thickness of the clip wall, x.

$$N = D\frac{(C_S - C_O)}{x} \qquad \text{(Equation 1.2)}$$

Molar flux is the flow of moles per second per unit surface area (mol/s-m$^2$), therefore, it must be multiplied by the cross-sectional area of the flow path. In this case, it is the circular cross-sectional area of the drug delivery channel, $A_{CHAN}$. It is also divided by the initial mass of drug loaded, $M_o$, to achieve a normalized release rate in terms of percent release ($dQ_{CHAN}/dt$).

$$\frac{dQ_{CHAN}}{dt} = N\frac{A_{CHAN}}{M_o} \qquad \text{(Equation 1.3)}$$

Combining equations 1.2 and 1.3, we arrive at a final equation describing percent release rate.

$$\frac{dQ_{CHAN}}{dt} = D\frac{A_{CHAN}}{M_o}\frac{(C_S - C_O)}{x} \qquad \text{(Equation 1.4)}$$

### 5.3.2 *Release from Porous Walls*

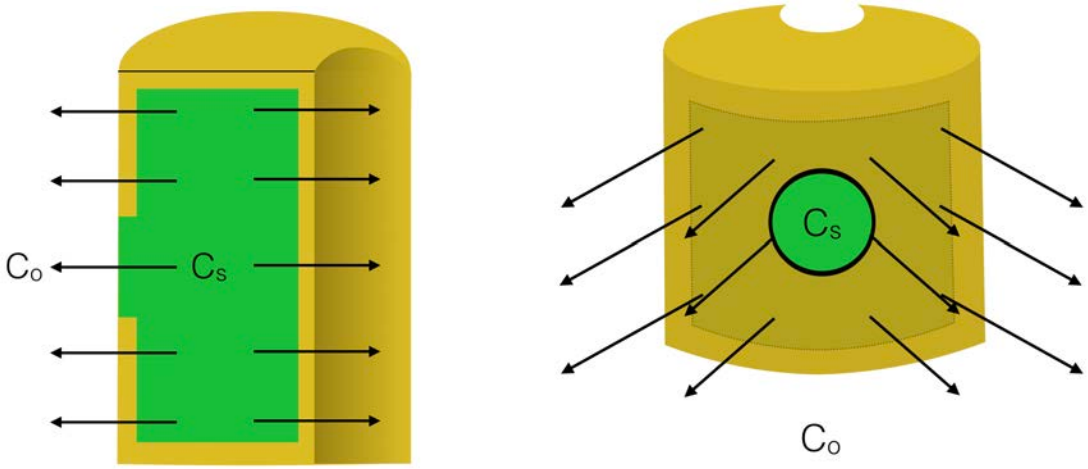


Figure 14: Release through the porous walls is constant. Concentration within the clip is constant as drug is constantly dissolving, while outside of the clip is an infinite sink (drug concentration is 0).

Release from the porous walls of the clip is similar to the previous model in that concentration of drug inside the reservoir is $C_S$ and the concentration outside is 0. However, the geometry of the diffusion path in this case is cylindrical instead of linear. Using these two assumptions, we can apply a steady state Fickian diffusion model considering radial diffusion.

$$0 = -D\frac{1}{r}\frac{\partial}{\partial r}\left(r\frac{\partial c}{\partial r}\right) \qquad \text{(Equation 2.1)}$$

To analytically solve this equation, a set of boundary conditions must be applied. Considering the clip as a hollow cylinder, we define two radii: the inner radius within the clip wall, $R_i$, and the outer radius outside the clip wall, $R_o$ (Figure 15). During release, we assume that the concentration at $R_i$ is equal to the solubility of drug, $C_S$, while the concentration at $R_o$ is zero. Applying these conditions allows integration of equation 2.1.

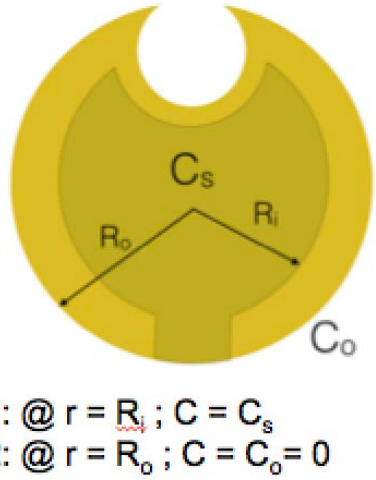


Figure 15: Boundary conditions used to analytically solve Equation 2.1.

$$\frac{dc}{dr} = \frac{C_S}{r \cdot \ln\left({}^{R_i}/_{R_o}\right)} \qquad \text{(Equation 2.2)}$$

Equation 2.2 essentially describes the radial concentration gradient. This can be plugged into Fick's first law, which relates molar flux, N, to the concentration gradient by the diffusion coefficient.

$$N = -D\frac{dC}{dr} \qquad \text{(Equation 2.3)}$$

$$N = -\frac{D}{r}\frac{C_S}{\ln\left({}^{R_i}/_{R_o}\right)} \qquad \text{(Equation 2.4)}$$

As in the previous case, molar flux is per unit surface area, therefore, it must be multiplied by cylindrical surface area of the clip, $A_{CYL}$. It is then normalized to the initial mass of loaded drug to achieve percent release.

$$\frac{dQ_{CYL}}{dt} = \frac{D}{r \cdot M_o}\frac{C_S \cdot A_{CYL}}{ln\left({}^{R_i}/_{R_o}\right)} \qquad \text{(Equation 2.5)}$$

A final consideration of the model is that the drug is diffusing through a porous material, therefore, release rate will be slower relative to diffusion through a pure liquid medium. Two unit-less terms are introduced that correct for this: percent porosity, ε, and tortuosity, τ.

$$D_{Eff} = -D_o\frac{\varepsilon}{\tau} \qquad \text{(Equation 2.6)}$$

Where $D_O$ is the diffusion coefficient of the drug in a pure liquid medium and $D_{Eff}$ is the corrected diffusion coefficient [48, 49]. ε was measured using μCT (see section 5.2), while τ is an empirically-derived constant. For a packing of spherical pores, τ is approximately 3 [48, 49]. Combining equations 2.5 and 2.6, the final equation for percent release from the porous cylindrical walls of the clip is:

$$\frac{dQ_{CYL}}{dt} = \frac{D_o\varepsilon}{r \cdot \tau \cdot M_o}\frac{C_S \cdot A_{CYL}}{ln\left({}^{R_i}/_{R_o}\right)} \qquad \text{(Equation 2.7)}$$

### 5.3.3 *Combining Release Modes*

Because drug will release from the clip both through the porous walls and through the drug release channel, the true release rate is the sum of both of these rates.

$$\frac{dQ_T}{dt} = \frac{dQ_{CHAN}}{dt} + \frac{dQ_{CYL}}{dt} \qquad \text{(Equation 3.1)}$$

Thus, a final percent release rate can be determined by combining equations 1.4 and 2.7 into 3.1.

$$\frac{dQ_T}{dt} = D_o \frac{A_{CHAN}}{M_o} \frac{(C_S - C_O)}{x} + \frac{D_o \varepsilon}{R_o \cdot \tau \cdot M_o} \frac{C_S \cdot A_{CYL}}{ln\left({R_i}/{R_o}\right)} \qquad \text{(Equation 3.2)}$$

## *4.3 Model Validation Release Experiment*

To validate the model, a drug release experiment was performed. Approximately 120 g of powdered methylene blue (MeB) was loaded into two clips. MeB was selected as the simulated drug because it is well characterized in the literature and has solubility properties similar to our target antibiotics. Both clips were submerged in 200 mL of PBS at 37° C under moderate shaking (90 rpms). Media was refreshed every 30 minutes and a small aliquot was collected for analysis. Aliquots were plated on a flat-bottom 96-well plate and scanned in a TECAN Infinite® M1000 spectrophotometer (λ=600 nm). Concentrations were measured against a standard curve ($R^2$>0.99). Release data was fit to a linear regression and the slope of the regression line was plugged into the model (equation 3.2) to back-calculate the diffusion coefficient, $D_O$.

## *4.4 Results*

Release experiment was performed in duplicate and the data was fit to a linear regression, which revealed 3.27% release per hour over the first three hours ($R^2$=0.996).

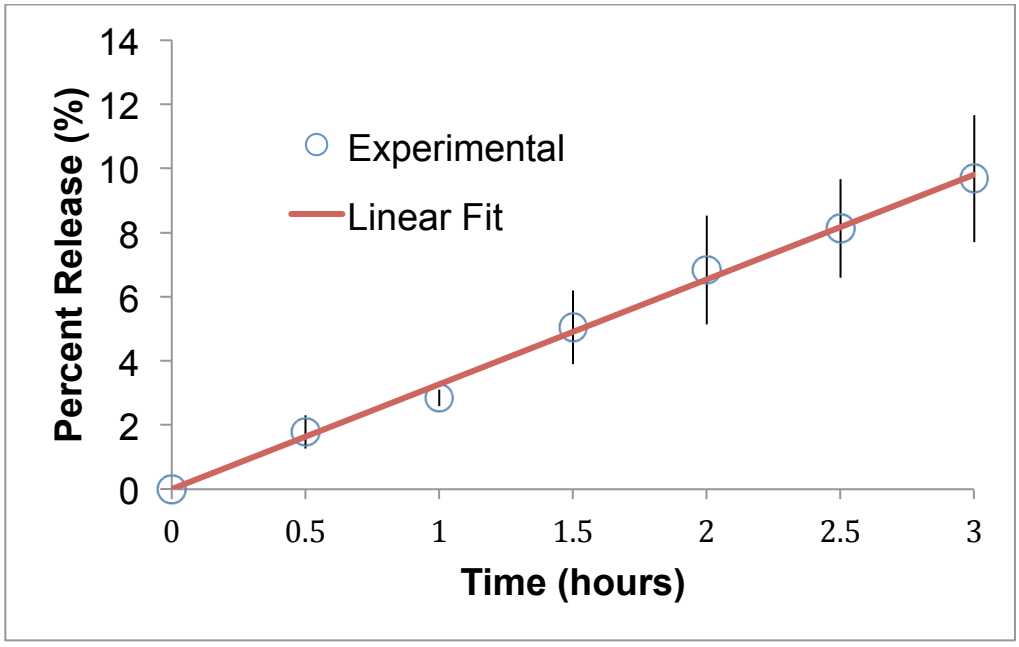


Figure 16: Release results were fit to a linear regression ($R^2$=0.996), revealing a 3.27% release rate over the first 3 hours.

This percent release rate was plugged into equation 3.2 of the model along with parameters from the Solidworks design ($A_{CHAN}$, $M_O$, x, $A_{CYL}$, $R_O$, $R_i$) and the porosity of the SLS PEEK material (ε, measured via μCT). The solubility of methylene blue in water was found from the literature [50] and the tortuosity factor (τ) was approximated as that

of a sphere pack [48, 49]. The equation was then used to calculate the diffusion coefficient ($D_o$) of methylene blue in water.

Table 2: Parameters used in the mathematical model validation.

| | Parameter | Description | Value |
|---|---|---|---|
| Experimental | $dQ_T/dt$ | Release Rate | 3.27% /h |
| Solidworks | $A_{CHAN}$ | Cross-Sectional Area of Channel | 7 $mm^2$ |
| | $A_{CYL}$ | Cylindrical Surface Area of Clip | 339 $mm^2$ |
| | x | Wall Thickness | 1.5 mm |
| | $R_O$ | Outer Radius of Clip | 6 mm |
| | $R_i$ | Inner Radius of Clip | 4.5 mm |
| | $M_O$ | Initial Mass of Loaded Drug | 120 mg |
| μCT | ε | Porosity | 0.38 |
| Literature | $C_S$ | Solubility of MeB in Water | $4.36\times10^7$ $mg/m^3$ |
| | τ | Tortuosity Factor | 3 |

Ultimately, a diffusion coefficient of $7.16\times10^{-8}$ $m^2/s$ was calculated. However, looking at the release profile extended over ten hours, release rate accelerates at 3 hours and diverges from the model (figure 17).

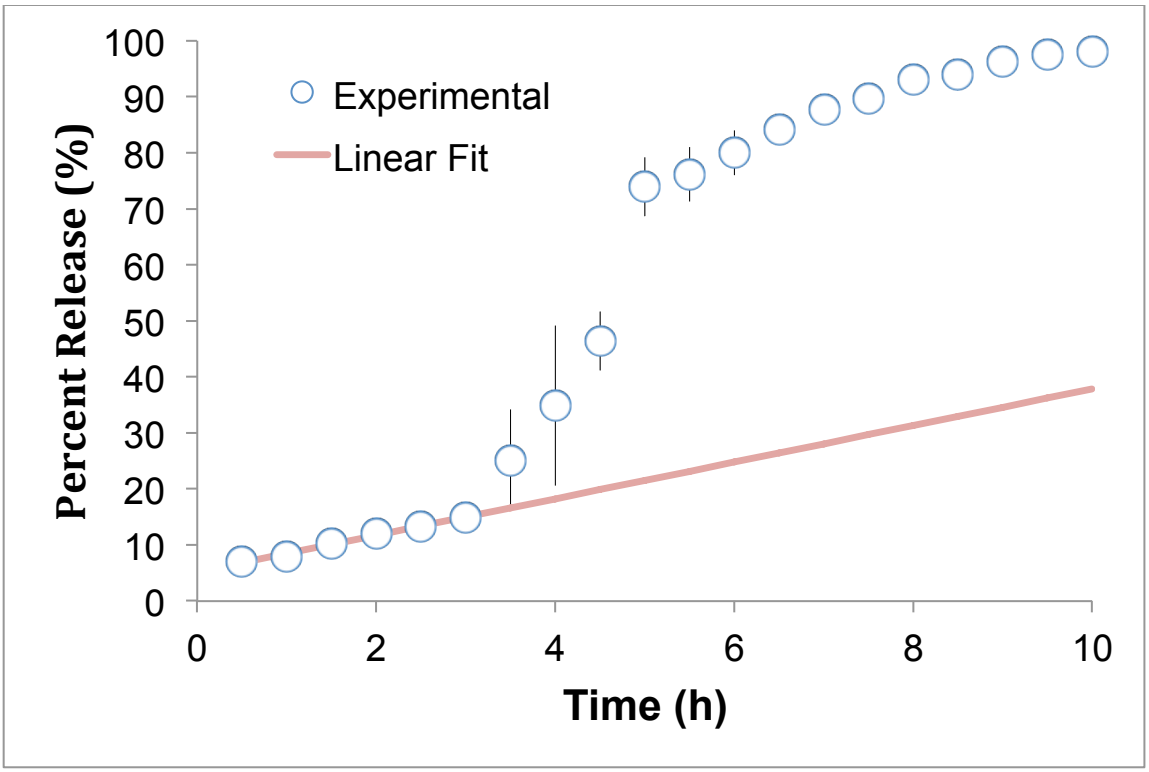


Figure 17: Release profile extended over 10 hours shows divergence from model at 3 hours.

This accelerated release proceeds from hour 3 to 5, then release slows again and asymptotically reaches 98% release by 10 hours.

## *4.5 Discussion*

The final model (Equation 3.2) predicts a linear release profile governed by dimensions of the clip, physical properties of the loaded drug, and properties of the porous SLS PEEK material. Release over the first three hours fit very well to a linear regression ($R^2$=0.996), which showed a release rate of 3.27 % per hour (Figure 16). This was used to

back-calculate the diffusion coefficient for MeB, $7.16\times10^{-8}$ $m^2/s$, which is within the same order of magnitude as reported diffusion coefficients for MeB in water. Agreed upon values for diffusion of MeB range from $5.5 \times 10^{-8}$ $m^2/s$ to $0.5 \times 10^{-9}$ depending on experimental conditions [51, 52, 53].

Table 3: Previously-determined values of the diffusion coefficient of methylene blue.

| D ($m^2/s$) | Temperature (°C) | Source |
|---|---|---|
| $5.05 \times 10^{-8}$ | 32 | Vadievelan et. al |
| $1.34 \times 10^{-9}$ | 30 | Sakar et. al |
| $0.83 \times 10^{-9}$ | 25 | Leasit et. al |

The diffusion coefficient I have derived is slightly higher than values reported in the literature, most likely because of my experimental conditions. First, moderate shaking during incubation introduced a small amount of convection, which would accelerate dissolution and release. This was employed to better simulate sink conditions experienced *in vivo*, in which drug would be immediately transferred away from the clip via the vascular system. Moreover, all of these diffusion coefficients were found at temperatures lower than 37° C, which was the temperature at which my release experiment was performed to simulate body conditions. Increased temperature is known to accelerate diffusion, which would lead to a higher diffusion coefficient. Despite these slight differences in experimental conditions, the diffusion coefficient derived here is comparable to literature values, adding support to the validity of the model.

This model is initial evidence that release occurs through the porous walls of the clip and the drug release channel. For reference, when performing the same back calculation for $D_o$ using equation 1.4, which assumes release only occurs through the drug delivery channel, $D_o$ is equal to 5.36 x $10^{-7}$ $m^2/s$. This $D_o$ is one to two orders of magnitude from the literature values for diffusion of methylene blue through an aqueous medium, which is added evidence that this is not the only drug-delivery route. However, this initial validation needs to be followed up with a few more release experiments to confirm validity. To further validate the model, one could test release out of the same clip design, made from a variety of porous PEEKs and a completely non-porous PEEK. What I would expect to see is a correlation between release rate and percent porosity since they are positively correlated according to the model. I would expect the non-porous material fit best to equation 1.4.

At three hours release accelerates, diverging from the linear model (figure 17). If the model accurately describes release for the first three hours, what changes at hour three to accelerate release? Examining the parameters in Table 2, it is unlikely that the solubility of MeB (a physical property of the molecule) changes over time. Likewise, the pore structure of the SLS PEEK material and the dimensions of the clip are unlikely to change since PEEK does not swell. Thus porosity, tortuosity and the clip dimensions probably do not vary over time.

My current hypothesis is that the solute-solvent surface area ($A_{CHAN}$ and $A_{CYL}$) changes at hour three due to particle dispersion. An assumption of the model is that the MeB powder

is well packed within the reservoir, behaving like one solid instead of an aggregation of particles. This allowed us to approximate the solute-solvent surface area as the cross-sectional area of the drug delivery channel and the cylindrical surface area of the clip. However, if particles disperse, the solute-solvent surface area drastically increases. Because release rate is proportional to the solute-solvent interface, when particles disperse, release rate increases.

This accelerated release was observed from 3 to 5 hours, then release slows once again. At this point, the particles within the bulk of the reservoir that were not as densely packed have probably all been depleted. The release from hours 5 to 10 is probably from particles that are stuck against the sides of the reservoir wall, which would be more compact and less prone to dispersion. This segment of the release profile is also non-linear as MeB depletes and release asymptotically approaches 98% at 10 hours.

Despite these limitations, a key take away of the model is that release does proceed from the porous walls. Porosity analysis in specific aim 1 (Figure 11) revealed spherical pores distributed through the SLS PEEK material. It was important to characterize porosity as equation 3.2 of the model shows that release rate is governed by percent porosity ($\varepsilon$) and tortuosity factor ($\tau$).

Percent porosity is merely the percent of the volume that is empty space within a given volume (in this case the volume of the clip). Tortuosity, is less tangible as it is an empirically-derived correction factor. While tortuosity in two dimensions is defined as

the ratio of length to curvature of a channel, translating that definition to three dimensions becomes difficult to measure. Instead of attempting some sort of physical measurement, tortuosity of 3-dimensional pore networks has been empirically derived by back-calculating the diffusion coefficients from release experiments through porous materials [54]. The major finding from these experiments is that materials of comparable percent porosity will exhibit different release rates based on the geometry of their pores [54]. To correct the diffusion coefficient for these changes, the tortuosity factor is applied. For example, a network of spherical pores has a $\tau$ of 3, but a cylindrical network (such as a capillary bed) has a $\tau$ between 1.14 and 1.5 [55]. The SLS PEEK pores were assumed to be of a spherical geometry based on cross-sectional images (Figure 11 (A)).

The other major conclusion from this experiment is that release will occur over 10 hours for an uncoated clip. The application of any membrane will inherently obstruct the diffusion path and slow release. We want complete release within 24 hours of sonication, therefore, this experiment shows that the membrane cannot prolong release more than 14 hours.

# 5. SPECIFIC AIM 3: Membrane Development

## *5.1 Aim Description and Hypotheses*

The membrane must serve two, seemingly conflicting, functions. It must be thick enough to retain drug within the reservoir for 7 days post-operatively but must be thin enough to release the drug when ultrasound is applied. I hypothesize that:

1. The membrane thickness can be varied.
2. The optimal membrane thickness can be achieved, which holds drug for 1 week, but ruptures in response to ultrasound.

## *5.2 Ultrasound-Triggered Drug Delivery*

Ultrasound (US)-triggered drug delivery is currently being investigated for a wide variety of treatments, including cancer chemotherapy, gene delivery, and as a way of bypassing the blood brain barrier. In general, all US-triggered drug delivery involves a hydrophobic drug carrier encapsulating a payload of drug and a small volume of air. When submerged in an aqueous medium, this carrier exists at a constant volume. However, the application of US to the medium induces pressure oscillations, which cause the bubble to expand and contract in a process known as cavitation [56]. If the amplitude of the pressure oscillations surpasses the cavitation threshold, the carrier will expand and then implode, causing the bubble to fragment and the encapsulated drug to escape [57].

Current popular drug carriers include PLA and PLGA microspheres, micelles, and lipospheres, which range from nanometers to micrometers in diameter [58]. Traditionally, large quantities of these carriers are administered via intravenous infusion. Local drug delivery is achieved at the site of sonication, where bubbles in the area are cavitated; bubbles that are not exposed to US remain intact and are excreted through the renal system [59].

It has also been recently demonstrated that US can increase the permeability of a membrane. This is currently being investigated as a method for bypassing the blood brain barrier, by temporarily increasing permeability of the brain's endothelial cells [56]. In an in vitro study, a monolayer of endothelial cells were exposed to lipid microbubbles and sonicated at an amplitude of 500 kPa and frequency of 1.5 MHz for 5 s [60]. Although the physical mechanism is not fully understood, it appears that the expansion of the microbubbles near cell membrane surface temporarily displaces the plasma membrane, allowing endocytosis of microbubbles [56]. Cells exposed to ultrasound experienced significantly more permeability to a dye for up to 3 hours relative to unsonicated controls [60].

### *5.3 Alternative Triggered Drug Delivery Techniques*

Drug delivery triggers can be divided into two major categories: externally-applied triggers, and local environment triggers. Ultrasound is an example of an external trigger

which can be applied by the physician, thus affording the clinician precise temporal control over drug release. Another external trigger is heat, which is being investigated to release chlohexidine from styrene and n-butyl(meth)acrylate co-polymer films [61]. At 48° C this polymer releases the antibiotic in a burst, much like the ultrasound release clip, and could be applied as a surface coating, mitigating the need for the clip attachment. However, heating the local tissue to 48 ° C for more than 20 seconds caused tissue damage. Near infrared (NIR) triggered photodegradable polymers can also be applied to surfaces [62]. This coating can actually be applied using layer-by-layer assembly (dipping) which is a similar technique used here to apply the PLA membrane. The NIR trigger is not cytotoxic and the thickness and morphology of the coating can be tuned. The photodegradation technology also rely on the presence of heavy metals such gold and silver, which have their own antimicrobial effects.

Local environment schemes rely on changes to the local tissue environment to trigger drug release. These drug carriers can be considered self-defensive since they respond to local bacterial activity to trigger release. Polymeric cross-linkers have been designed, which degrade in responsive to changes in local pH caused by bacterial activity [63]. These can be small microsphere carriers or layer-by-layer film deposits on polymeric substrates [64]. These films show remarkable stability, retaining antibiotic for many months post-implantation and, therefore, are a long term option in managing local infection. However, an area of concern with these approaches is that by the time bacteria proliferate enough to trigger release, the biofilm may have already developed antibiotic recalcitrance.

A final drug-delivery method that merits review here is degradation-controlled drug delivery. Theoretically, a membrane could be designed with the same retention function that has been laid out here. However, instead of release being triggered with ultrasound, the membrane could erode at the water-membrane surface until releasing drug at one week. This degradation-controlled system would require a hydrophobic polymer that undergoes surface erosion such as polyhydroxyalkanoates, polyanhydrides, or polyacetals [65]. This approach lacks the external ultrasound trigger, however, which would also disrupt the biofilm and increase its antibiotic susceptibility. Moreover, many of the degradative byproducts of these polymers are inflammatory, which may prolong wound healing.

### *5.4 Poly(lactic acid)*

Poly(lactic acid) (PLA) is commonly employed in drug delivery applications such as microspheres [66]. Its extreme hydrophobicity is often used to delay drug release, preventing the encapsulated drug from mixing with the aqueous environment of the body. Release from PLA is often degradation-controlled, as PLA readily undergoes hydrolytic degradation [67]. This involves bulk erosion, in which, ester bonds throughout the polymer backbone undergo chain scission [67]. Relative to other popular drug carrying polymers PLA degrades very slowly, showing 90% retention in vivo over 15 weeks [68]. PLA's slow degradation is ideal for the drug delivery clip, which relies on a solid hydrophobic membrane for 1 week. The primary byproduct of degradation is lactic acid,

which is naturally produced by human cells during anaerobic respiration. However, the build up of lactic acid *in vivo* has been shown to cause chronic inflammation [68].

### *5.5 Membrane Development*

Clips were loaded with approximately 120 mg of MeB and PLA (75-120 kDa) membranes were applied via submersion in PLA-chloroform ($CHCl_3$) solutions. All clips were submerged in a PLA-$CHCl_3$ and dried for 10 minutes in between coatings. One group of clips, was coated 5 times in a PLA-$CHCl_3$ solution of 50 mg/mL (5-50 group). Another set of clips were submerged ten times in 50 mg/mL solution (10-50 group). A final set of clips was submerged five times in a PLA-$CHCl_3$ concentration of 250 mg/mL (5-250). After coating, all clips were left out over night to ensure complete solvent evaporation.

Two batches of clips were made. In batch one, two of each clip was manufactured. In batch two, three of each clip was manufactured. The only difference in manufacturing between the two batches was in drying method. To dry the clips of batch one, the clips were set on their side on the bench top (figure 18-A), which created a significant contact area between the clip and the bench top.

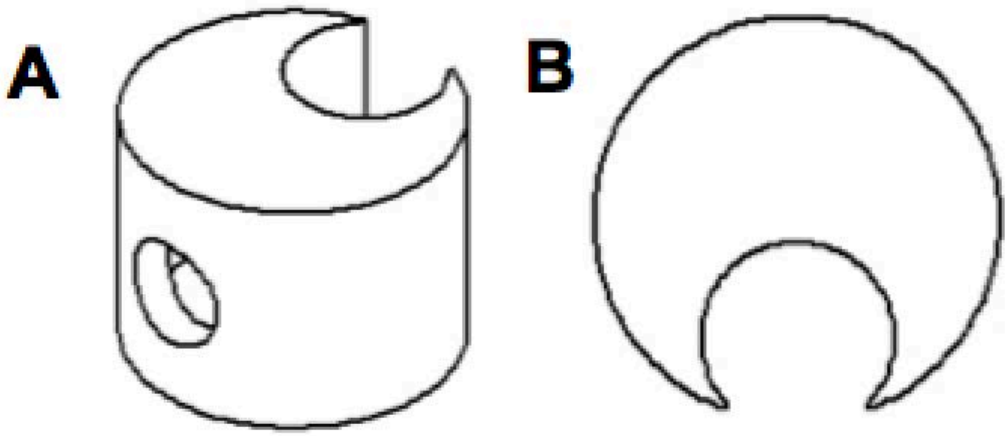


Figure 18: (A) Batch one clips were dried on their tops and were difficult to remove from the bench top after drying. (B) Batch two clips were dried on their flanges, minimizing interfacial area with the bench top.

After drying, it was rather difficult to remove the clip from the bench top and significant force had to be applied with tweezers to remove the clip from the bench top. This may have disrupted the membrane and created defects that affect performance. To minimize membrane disruption after drying, batch two clips were dried on their flanges (Figure 18-B) to minimize the surface of the clip in contact with the bench top. Mass of clips was measured before and after coating. The difference between these mass measurements represents the amount of PLA deposited on the clip.

### *5.6 Membrane Retention-Release Experiment*

Clips were attached to 5.5 mm stainless steel rods (Grade 316-L), which is the grade of metal used in most spinal fusion rods. Clips and rods were then submerged in 200 mL of

PBS at 37º C under moderate shaking (90 rpms). Media was refreshed every 24 hours and an aliquot was stored for later analysis.

At the end of 1 week, ultrasound was applied to the medium containing the rod and clip for 20 minutes using a SonixRP Scanner with an L4-9 probe (Analogic Ultrasound, Richmond, BC, Canada) transmitted at 5 MHz and 3 MPa (peak-to-peak) acoustic output pressure. Media was refreshed and collected 1, 2, 3, 6 and 24 hours after sonication. Aliquots were placed in a flat-bottom 96-well plate and scanned in a TECAN Infinite® M1000 spectrophotometer ($\lambda$=600 nm). Concentrations were measured against a standard curve ($R^2$>0.99). Release profiles before and after sonication were fit linear regressions and percent release rates were used to compare coatings.

### *5.7 Results*

Upon submersion in the PLA-$CHCl_3$ solution, some MeB leached from the clip into the solution, although this mostly occurred on the first submersion. After drying for 24 hours, the membranes were blue indicating that some MeB was trapped within the PLA. However, PLA was only visible on the surface of the 5-250 clips from either batch. There was no visible PLA deposited on the surface of the 5-50 or 10-50 clips, however, mass measurements taken before and after coating indicate that 86.5 mg of PLA was present on or in the 5-50 clips from batch one, and only 7 mg of PLA was present on those from batch 2. The 10-50 clips from batch one contained 161 mg of PLA and the 5-250 clips had 173.5 mg of PLA. This is in contrast to the 10-50 clips from batch 2, which only had 13 mg of PLA. Clips were imaged via SEM using the method described above in Aim 1.

All images were taken at 120 x to get an overview of the state of the material surface after coating. SEM images reveal that the 5-250 technique resulted in the thickest and most homogenous surface layer. In fact, the original morphology of the SLS PEEK material is no longer visible. 10-50 and 5-50 clips had PLA on the surface, however, pores were still visible throughout. All clips were attached to 5.5 mm steel rods prior to submersion in PBS, which simulates surgical attachment to a spinal fusion rod.

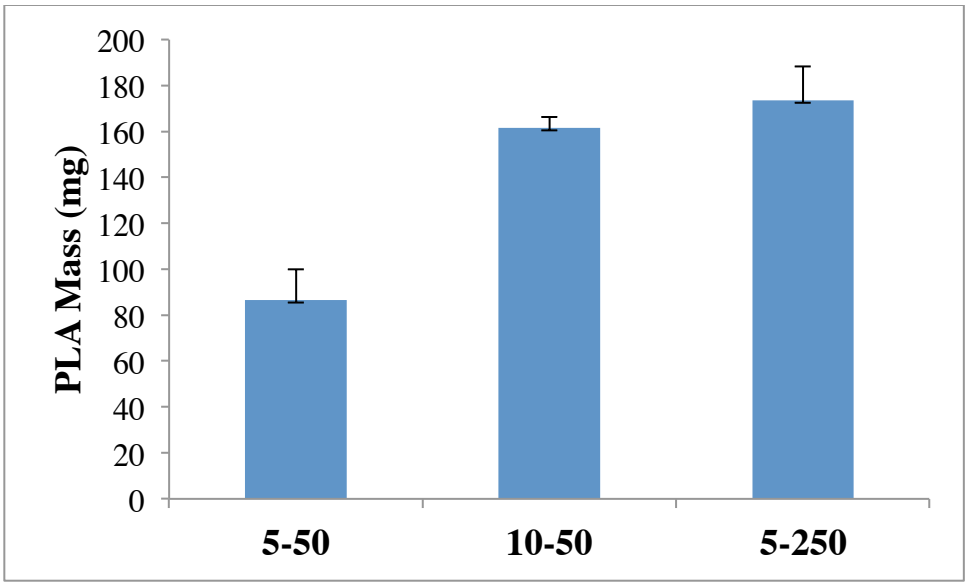


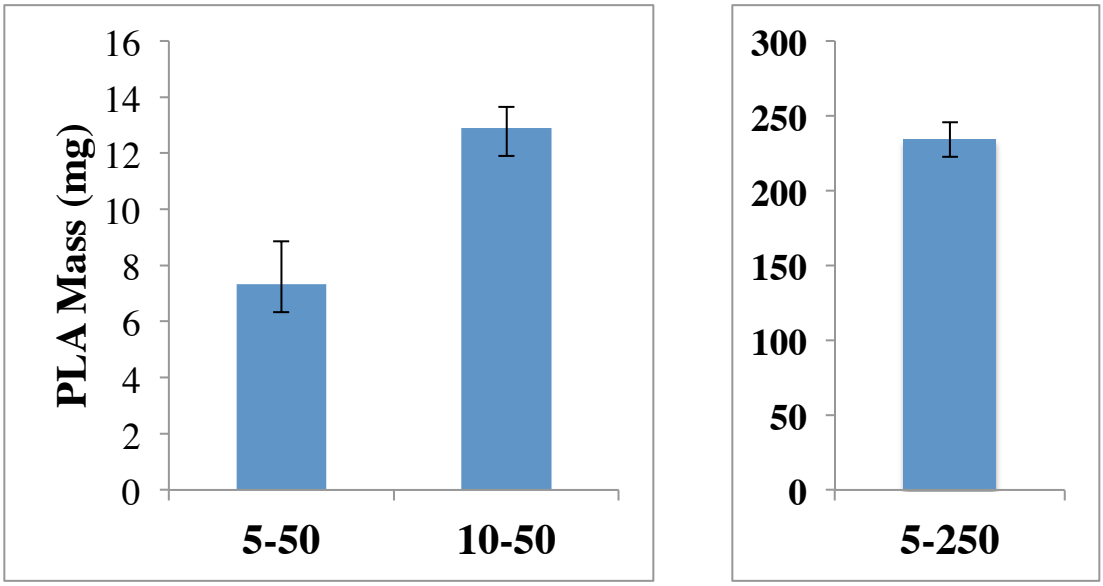


Figure 19: Mass measurements taken before and after coating. (Top) Measurements of the batch one clips show the 5-50 clips contained 80 mg of PLA, the 10-50 clips had 161 mg and the 5-250 clips contained 173.5 mg. (Bottom) An order of magnitude less PLA was deposited on the 5-50 and 10-50 batch two clips. However, 80 mg more PLA was deposited on the surface of the 5-250 clips of batch two than batch one.

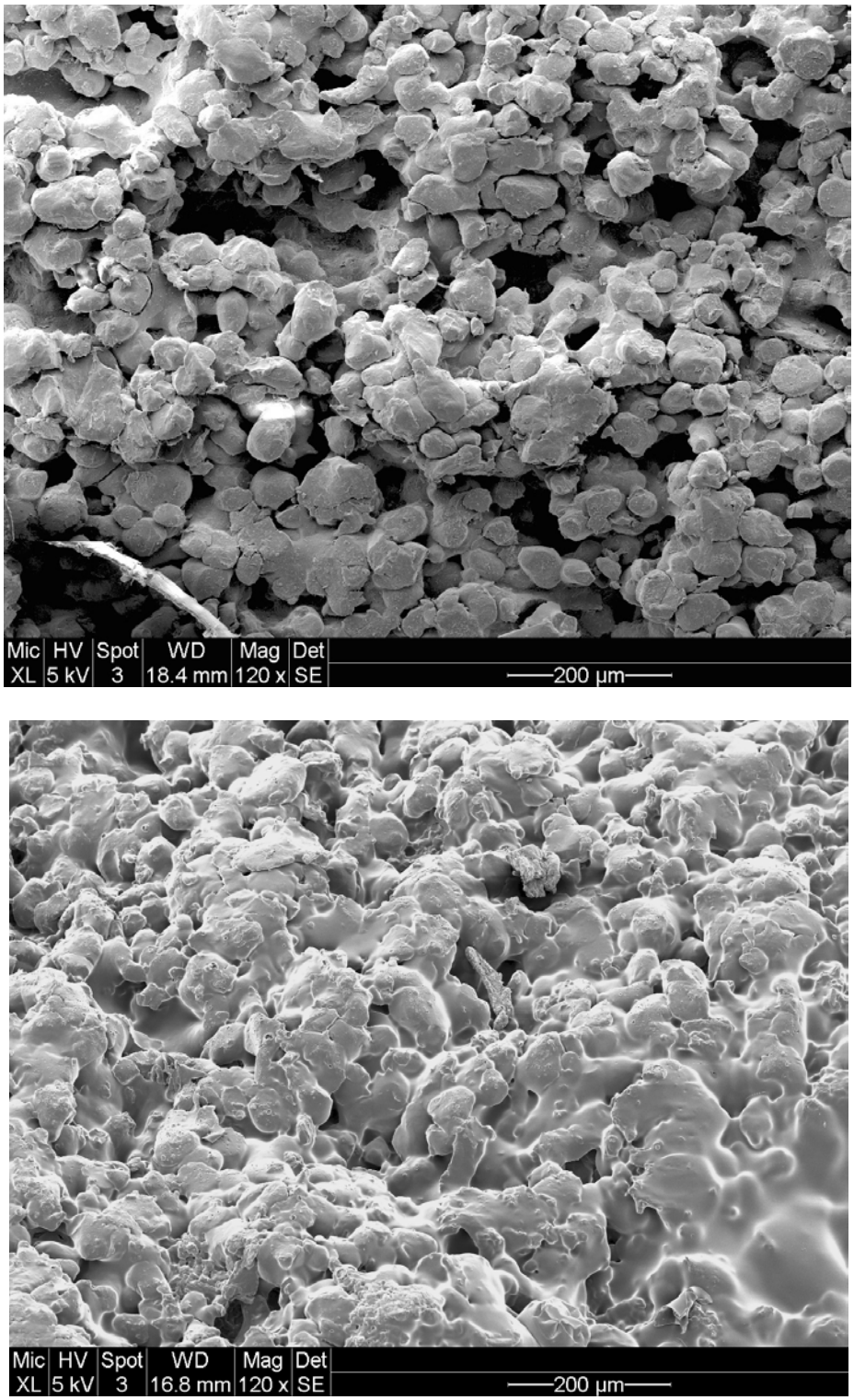


Figure 20: (Top) SEM image of the un-coated SLS PEEK material. (Bottom) The surface of the material coated with the 5-50 technique. PLA is deposited on the surface and within the pores, although pores are still visible.

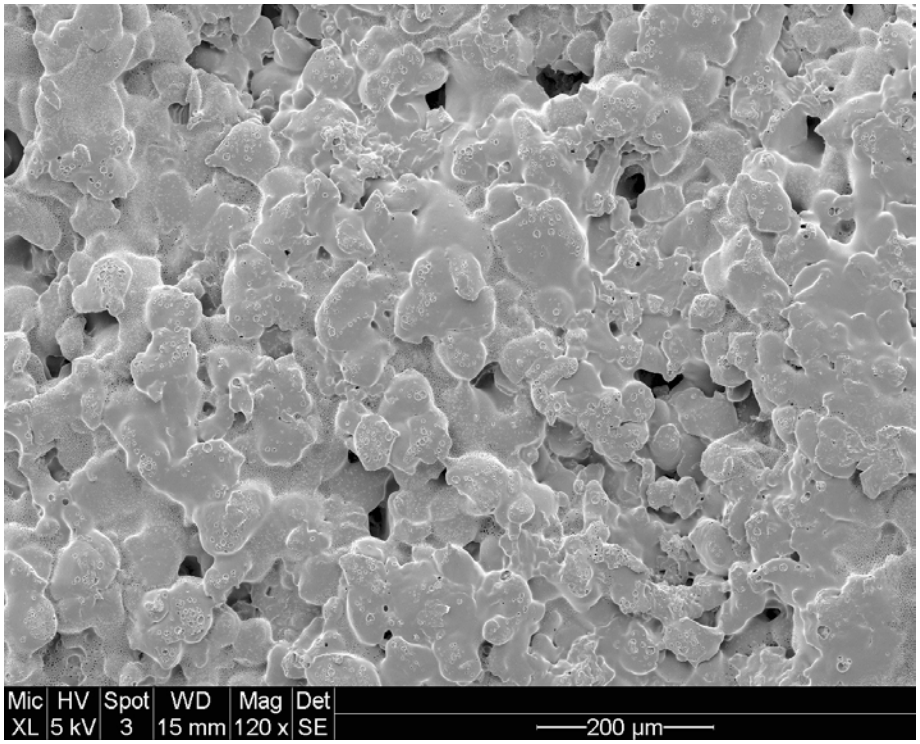


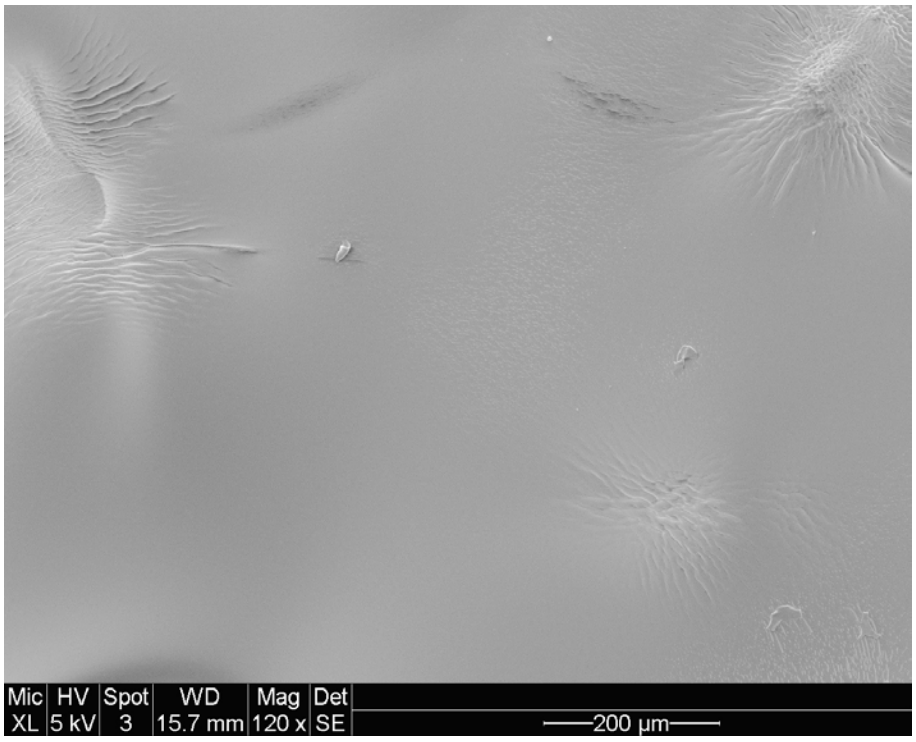


Figure 21: (Top) Surface of the 10-50 shows even more PLA deposition than the 5-50 technique, although pores are still visible through (Bottom) The 5-250 membrane is a thick layer that completely hides the original morphology of the SLS PEEK surface.

During the incubation period (up to day 7) of the batch one clips, the 5-250 clip leaked the least with only 19% of the MeB releasing. The 5-50 and 10-50 clips both allowed 38% release during the first week. All of these release profiles are seemingly linear.

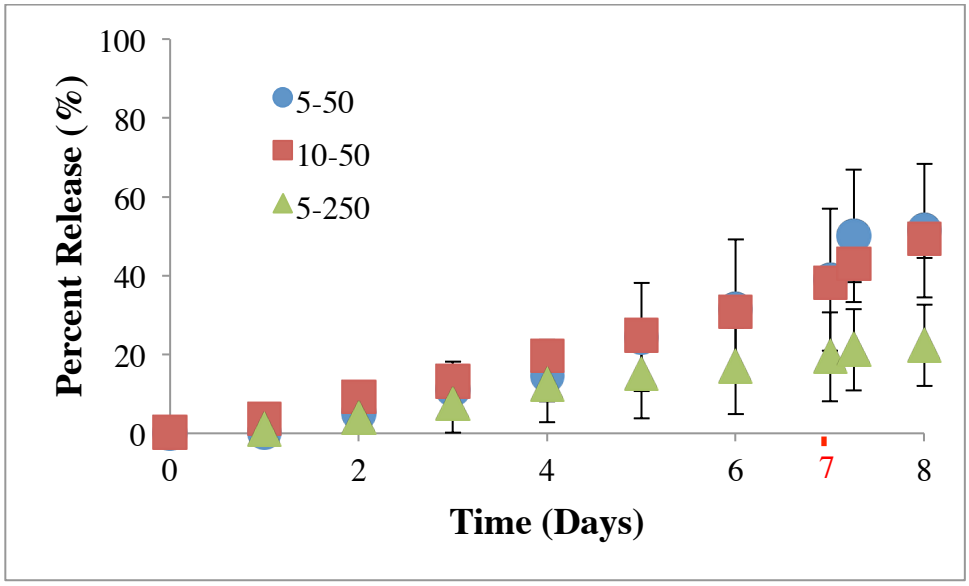


Figure 22: The 5-250 clips allowed for 19% MeB release over the first week, while 5-50 and 10-50 clips both allowed 38% release. Ultrasound was applied at day 7 and release was observed for an additional 24 hours.

Release profiles from before and after sonication were fit to linear regressions ($R^2$>0.59). 5-50 and 10-50 clips had comparable release rates (5.85 and 5.4 %/day, respectively) while 5-250 released 3% of its MeB per day for the first 7 days of incubation.

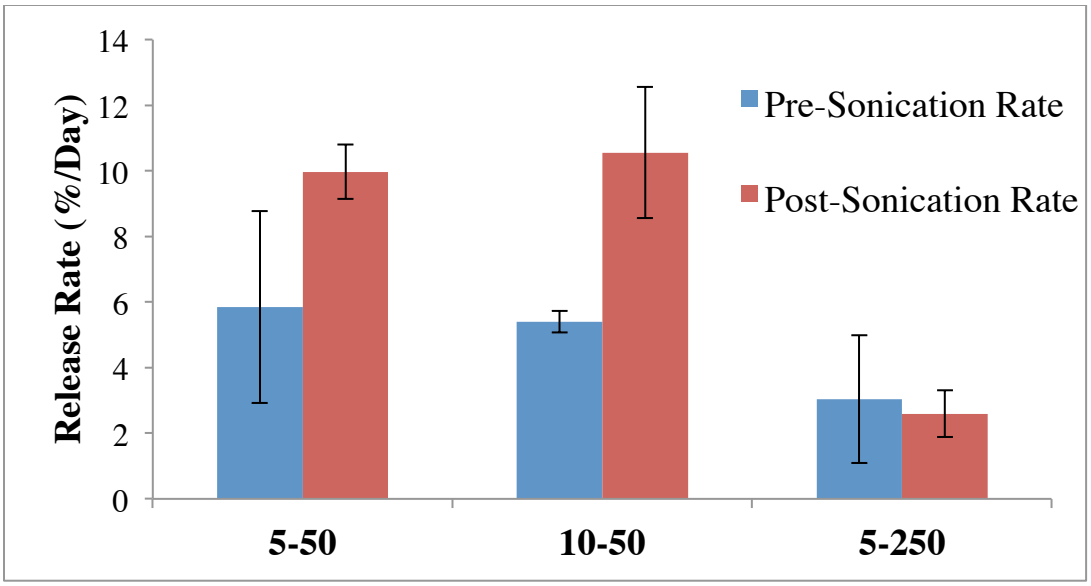


Figure 23: Pre-sonication release was fastest in the 5-50 group and slowest for the 5-250 group. Post-sonication, release was accelerated in the 5-50 and 10-50 groups. Release decelerated slightly in the 5-250 group.

Sonication accelerated release in the 5-50 clips to 10.0 %/day and accelerated release of the 10-50 clips to 10.6 %/day. Release from the 5-250 membrane slightly decelerated after sonication. Batch two release profiles were non-linear, instead showing an asymptotic profile during the 7-day incubation period (Figure 24 (top)). Ultimately 24% and 16% was released from the 5-50 and 10-50 clips respectively. The 5-250 clips showed less than 1% release during that period. After the application of ultrasound, 2% additional MeB release was achieved, and less than 1% from either the 10-50 or 5-250, seen in Figure 24 (bottom).

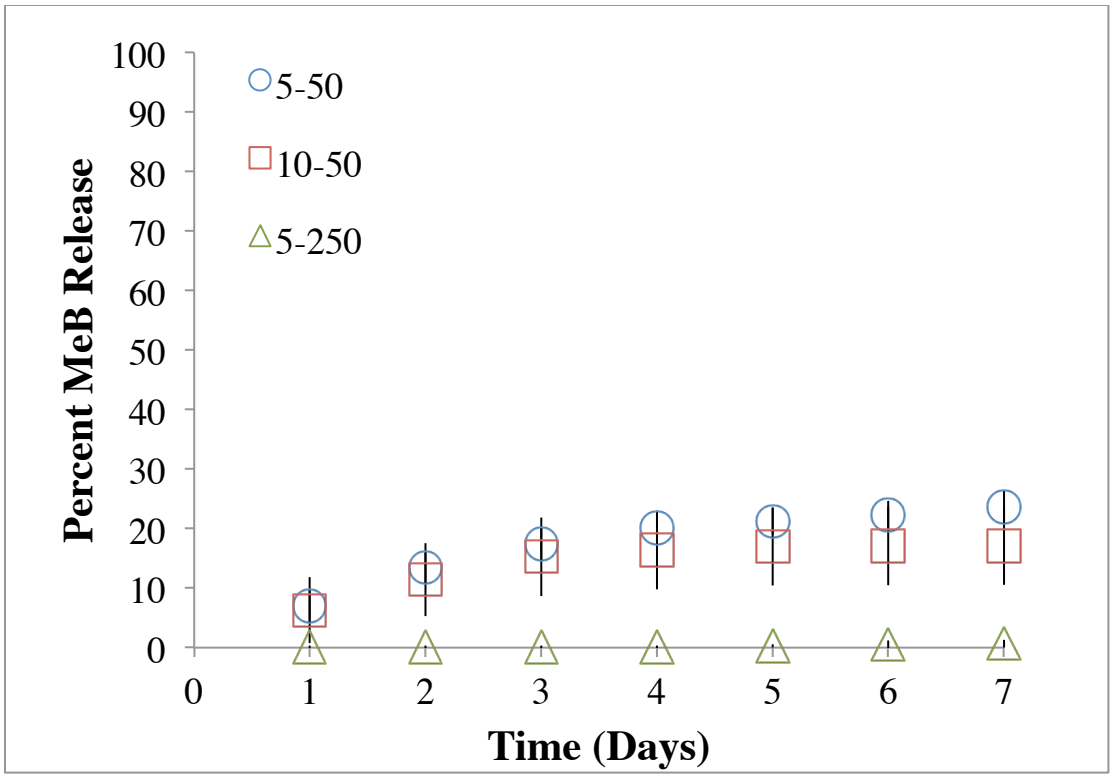


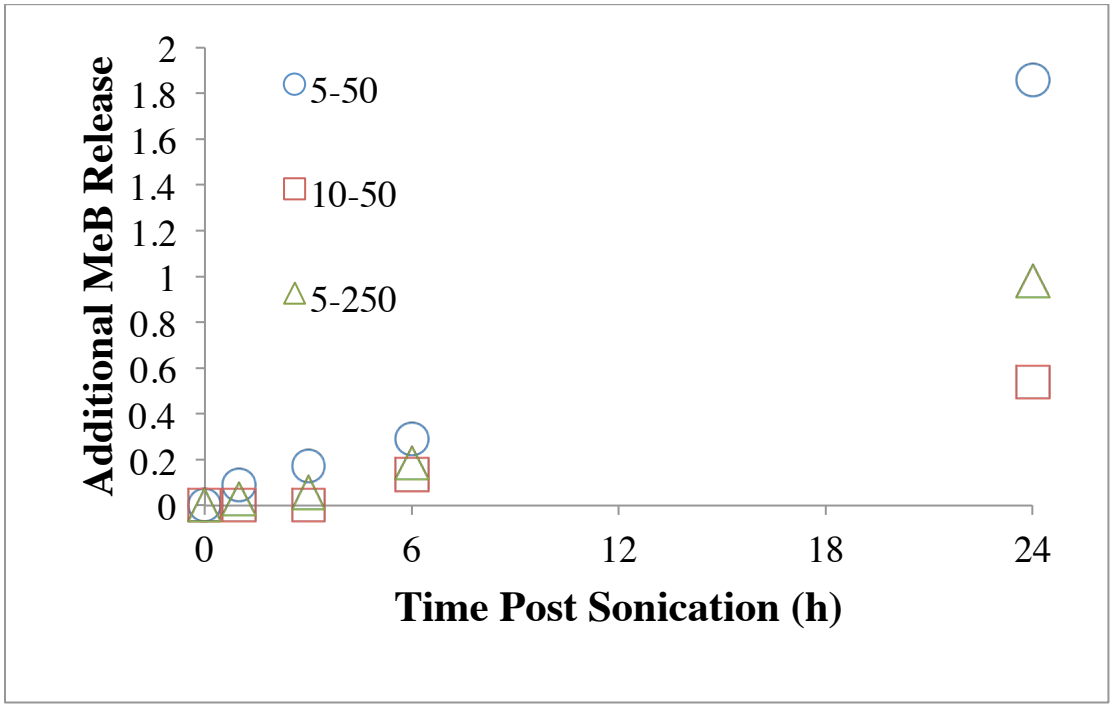


Figure 24: (top) Batch two release profiles during the first seven days of incubation. (bottom) Additional release following ultrasound triggering at the end of day 7.

## *5.8 Discussion*

Comparing the batch 1 and batch 2 manufacturing techniques, the first apparent difference is the amount of PLA deposited. The batch 2 5-50 and 10-50 clips had an order of magnitude less PLA than the batch 1 clips (figure 19). This may be because more PLA dripped off of the clips during drying in the batch 2 configuration. It may also be indicative of more efficient $CHCl_4$ evaporation. However, with the 5-250 clips we see the opposite trend, with more PLA deposited in the batch 2 process than the batch 1 process. No matter the explanation for these differences, these two batches highlight the variability of the manufacturing technique that must be minimized in future developments.

SEM imaging revealed that the 5-50 and 10-50 clips did have PLA on the surface, however, these membranes were thin and incomplete, with pores still distributed across the surface. The 5-250 clips had a thick surface layer that completely obscured the original morphology of the SLS PEEK surface. Based on these observations it is clear that the higher concentration PLA-$CHCl_3$ solution is more favorable for creating a surface membrane. This is probably because the more concentrated PLA-$CHCl_3$ solution is more viscous, enabling it to remain on the clip surface instead of infiltrating into the reservoir. These findings support my first hypothesis, in that the membrane thickness can be varied by varying the concentration of the PLA solution.

Over the first seven days of incubation, the membranes' ability to retain drug was tested. This represents the time between initial implantation and drug release. In the batch 1 assessment, the 5-250 clips showed the least leakage during this time, permitting 19% drug release versus the other clips' 38% drug release. What leakage did occur from the 5-250 clips, it was most likely from surface defects as seen in figure 25. Defects such as this were probably a result of handling during coating with tweezers.

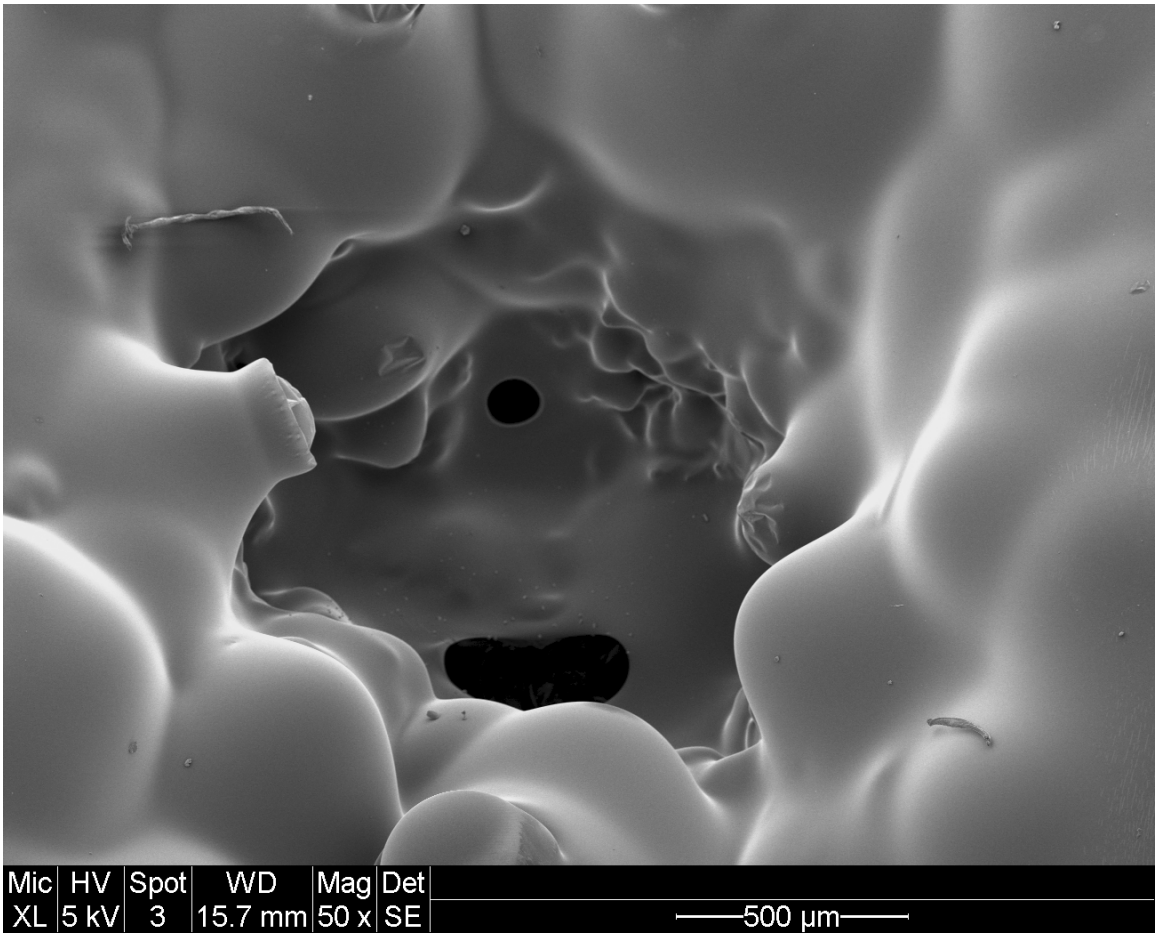


Figure 25: Defect observed on the surface of the 5-250 clip was probably the result of handling during and directly after coating.

Batch two clips, on the other hand, featured asymptotic release, which stabilized by day 7. The 5-50 clips in this batch only leaked 24% of their MeB, while the 10-50 clips only leaked 16%. The sustained release seen in the 5-50 and 10-50 clips is most likely due to MeB particles suspended in a PLA matrix due to infiltration of the 50 mg/mL PLA-$CHCl_3$ during coating. The 5-250 clips showed less than 1% leakage, indicating complete encapsulation of the reservoir. This indicates that the batch 2 drying configuration produced more complete membranes with less defects than the batch 1 clips.

A modest increase in release rate was observed post sonication from the 5-50 and 10-50 clips in batch 1. However, this may be the result of an increase in sampling rate during the post-sonication period. Every time media was sampled, the entire beaker was emptied and refilled with fresh PBS, which introduces some convection, possibly increasing dissolution and diffusion of the MeB. The increase in release rate may have been a result of this phenomena and not ultrasound. To test this, a control experiment should be done, to see if the accelerated release rate is observed in unsonicated clips sampled at the same rate. Application of ultrasound at the end of the incubation period had virtually no effect on release rate from any of the batch 2 clips, indicating that the membranes are too thick to rupture through cavitation (figure 24-bottom). Because these membranes are probably more complete than the batch 1 membranes, this is probably the more important finding to consider. Ultimately the 5-250 membrane fulfilled the retention function, more work needs to be done to achieve US-triggered release.

# 6 CONCLUSIONS and FUTURE WORK

To date, this is the first study using SLS PEEK as a drug delivery device. As demonstrated by the model, the SLS PEEK is porous enough to permit diffusion. In future iterations of the clip, it would be favorable to minimize material porosity so that release only occurs through the designed drug delivery channel. This would make the membrane easier to apply because it would only need to seal the drug delivery channel and not the entire clip. Porosity of SLS material is largely determined by particle fusion during sintering: circular smooth particles flow together more efficiently than irregularly-shaped particles [46]. Increasing laser energy density also makes the molten polymer less viscous, which promotes particle flowability as well [47]. This is an ongoing area of study with our collaborators at University of Exeter.

A major limitation of the clip design study is that clip attachment strength was not quantified. Further investigation is warranted to assess clip attachment while the rod undergoes cyclic loading. Stainless Steel spinal fusion rods can undergo flexion during normal activity and are shown to fatigue under cyclic mechanical loading [69], which could potentially cause loosening or migration of the clip. Moreover, wear at the clip-rod interface could generate inflammatory wear particles. To assess loosening and wear-particle generation, the clip could be attached to a fusion rod undergoing a cyclic loading test such as ASTM F1717-01. In this test, pedicle screws are drilled into polyethylene blocks, which simulate vertebrae, and fusion rods are loaded under physiologically relevant bending at 4 Hz over 2 million cycles. This test could also be done in

physiologically-relevant media, which could be collected and analyzed for PEEK wear particle generation. A method could be adapted from UHMWPE particle analysis, in which, particles are collected on a nuclepore filter, imaged via scanning electron microscopy and analyzed in ImageJ [70].

A model was derived using principles of Fickian diffusion and Noyes-Whitney dissolution to predict release from the clip. The model was validated over the first three hours of a release experiment from an un-coated clip. To confirm model validation, release experiments should be performed using clips manufactured in materials of various porosities. A positive correlation should be observed between release rate and material porosity, demonstrating that release proceeds faster from a more porous material. Moreover, release from a non-porous material should fit best to equation 1.4, which only takes into account release from the drug delivery channel.

Assuming the model is valid, it can be used to re-design the clip. One way to accelerate release from the clip would be to increase the number of drug delivery channels. To account for this in the model, the drug release term of equation 3.2 would be multiplied by N number of delivery channels. The cross-sectional area of the release channel could also be widened to accelerate release since it is directly proportional to release rate. Finally, the width of the walls could be made smaller, although, this can only be minimized to about 1 mm, which is the minimum resolution of the SLS manufacturing technique.

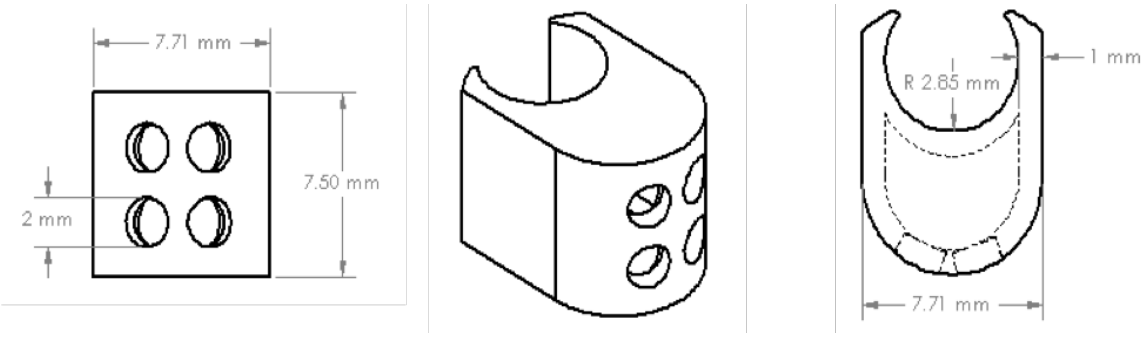


Figure 26: Possible second iteration of the clip, featuring more drug delivery channels and a smaller clip wall. According to the model, this clip would release drug faster than the previous clip version.

Figure 26 shows a second iteration of the drug delivery clip, designed with guidance from the model. The wall size has been minimized to 1 mm, which should provide less impedance for ultrasound waves to penetrate. This would also be a smaller diffusion path for the drug to release from. There are four, 2 mm drug delivery channels instead of one 4 mm channel. This should better distribute drug throughout the surgical site and will further accelerate release.

Membrane retention and release studies demonstrated a need for further membrane optimization to ensure the membrane can retain drug without leakage for one week and is also responsive to ultrasound-triggered release. One way to improve membrane retention is through better handling. To submerge the clips in PLA-$CHCl_3$ solution, I had to handle the clips with tweezers, which could potentially disrupt the membrane. Disruption could be minimized with longer dry cycles between dips. This would allow the previous coating to solidify and decrease the likelihood of disruption with tweezers. I hypothesize that with better handling, the 250 mg/mL coating could completely stop leakage. Assuming

this could be achieved, I could then try coating clips with incrementally less concentrated membrane solutions, which would decrease the membrane thickness and theoretically increase its responsiveness to ultrasound triggered release.

It is also understood that ultrasound's ability to increase the permeability of a membrane is increased with the addition of microbubbles near the membrane surface. These microbubbles cavitate, mechanically disrupting the adjacent membrane and temporarily increasing its permeability. This has been used to increase the diffusivity of the blood-brain barrier and to disrupt biofilm [36, 60]. While it would not be feasible clinically to inject microbubbles near the clip, it might be possible to trap more air in the membrane during coating. A homogenizer could be applied to the membrane solution before coating to make bubbles in the membrane solution, which might be retained after coating. I hypothesize that this entrapped air would make the membrane more responsive to ultrasound trigger.

Another major limitation of this study is that methylene blue was used to simulate an actual antibiotic. Once the membrane has been optimized, the device would probably be loaded with a combination of vancomycin and cefazolin to kill a broad range of gram-posotive and gram-negative bacteria. A bacterial challenge experiment could be performed, in which biofilm was grown on the surface of a stainless steel rod. The clip and rod would then be sonicated and incubated for an additional 24 hours while drug release proceeds. Bactericidal effect could be measured by detaching the bacteria from

the rod, plating and counting. This could also be compared to an unsonicated control to determine if there is any additional bactericidal effect using ultrasound.

While there is still more work to be done to optimize the clip, this study demonstrated initial feasibility of an ultrasound-triggered antibiotic release clip to lumbar posterior fusion surgery. This device has been thoughtfully designed to fit within current clinical antibiotic prophyalxis, which is a multi-step system that spans the peri-operative period. In the context of 4-stage biofilm formation, the first line of prophylactic defense is aimed at preventing bacteria from attaching to the implant surface. Antibiotics are administered prior to the operation and surgeons follow rigorous sterile surgical techniques to minimize bacterial exposure.

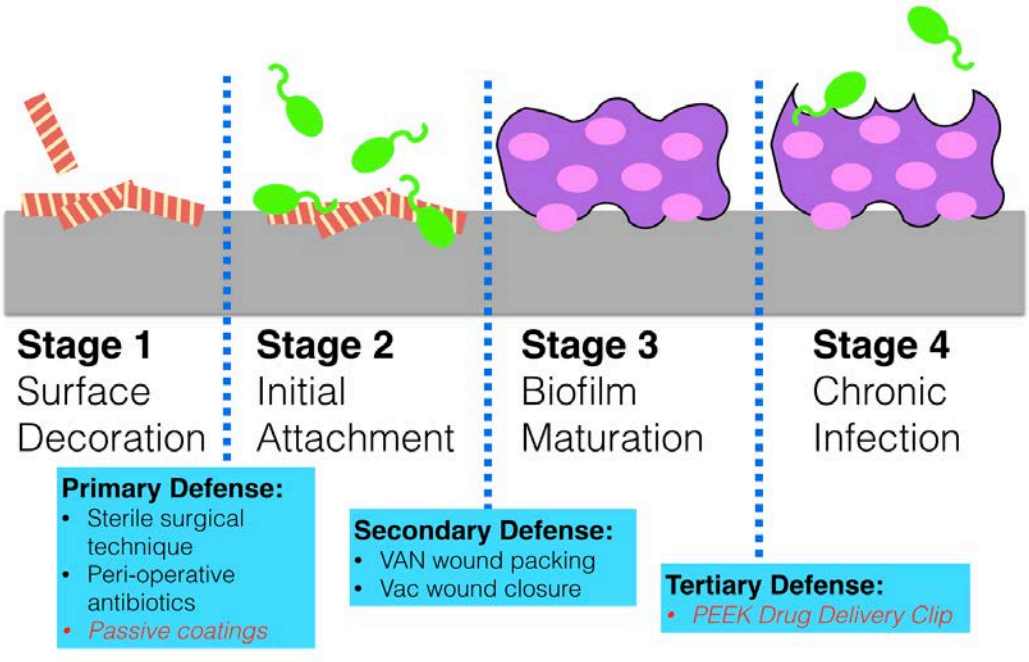


Figure 27: The PEEK clip will act as a tertiary defense system within the scope of standard clinical infection prophylaxis. It could also work in synergy with passive antimicrobial coatings currently under investigation.

While not currently in clinical use, non-fouling passive surface coatings are being investigated that would further prevent bacterial attachment to the implant surface. Of these, the most promising is silver, which inhibits a broad range of microbes and can be plasma sprayed onto the stainless steel fusion rods and pedicle screws. The second layer of defense is Vancomycin wound packing and vacuum wound closure. These have both shown promise at limiting infection and accelerating the formation of granulation tissue.

Finally, the SLS PEEK clip offers a tertiary layer of defense. Ultrasound will play two roles in this system: triggering release of antibiotic, but also disrupting the bacterial biofilm and increasing its susceptibility to antibiotics. This technology would provide clinicians with a third contingency in the fight against surgical site infection. Once implemented, it would surely lower the incidence of surgical site infection in lumbar fusion surgery.

**WORKS CITED**


1. Joseph, S. A., et al. (2008). "Lumbar spine fusion: Types, principles, and outcomes." Neurosurgery Quarterly **18**(1): 34-44.

2. Davis, W., et al. (2013). "Modern spinal instrumentation. Part 1: Normal spinal implants." Clinical Radiology **68**(1): 64-74.

3. Deyo, R. et al. (2004). "Spinal-Fusion Surgery - The Case for Restraint." The New England Journal of Medicine **350**(7): 722-726.

4. Gologorsky, Y., et al. (2014). "The Nationwide Inpatient Sample Database does not accurately reflect surgical indications for fusion." Journal of Neurosurgery-Spine **21**(6): 984-993.

5. Mannion, A. F., et al. (2014). "Development of appropriateness criteria for the surgical treatment of symptomatic lumbar degenerative spondylolisthesis (LDS)." European Spine Journal **23**(9): 1903-1917.

6. Deyo, R. A. (2012). "Point of View In Response to Spinal Fusion in the United States: Analysis of Trends From 1998 to 2008." Spine **37**(1): 77-77.

7. Kurtz, S., et al. (2011). "Infection Risk for Primary and Revision Instrumented Lumbar Spine Fusion in the Medicare Population." The Spine Journal **11**(10): S22-S22.

8. Nota, S., et al. (2015). "Incidence of Surgical Site Infection After Spine Surgery: What Is the Impact of the Definition of Infection?" Clinical Orthopaedics and Related Research **473**(5): 1612-1619.

9. Radcliff, K. E., et al. (2015). "What is new in the diagnosis and prevention of pine surgical site infections." Spine Journal **15**(2): 336-347.

10. Abdul-Jabbar, A., et al. (2013). "Surgical Site Infections in Spine Surgery Identification of Microbiologic and Surgical Characteristics in 239 Cases." Spine **38**(22): E1425-E1431.

11. Ishii, M., et al. (2013). "Postoperative deep surgical-site infection after instrumented spinal surgery: a multicenter study." Global Spine Kournal **3**(2): 95.

12. Kowalski, T. J., et al. (2007). "The management and outcome of spinal implant infections: Contemporary retrospective cohort study." Clinical Infectious Diseases **44**(7): 913-920.

13. Lambat, M. P., et al. (2013). "Impact of perioperative complications on clinical outcome scores in lumbar fusion surgery." Journal of Neurosurgery-Spine **18**(3): 265-268.

14. Dunne, J. W. M. (2002). "Bacterial adhesion: seen any good biofilms lately?" Clinical Microbiology Reviews **15**(2): 155-166.

15. Bjarnsholt, T. (2013). "The role of bacterial biofilms in chronic infections." Apmis **121**: 1-58.

16. Debabov, D. (2013). "Antibiotic Resistance: Origins, Mechanisms, Approaches to Counter." Applied Biochemistry and Microbiology **49**(8): 665-671.

17. Høiby, N., et al. (2010). "Antibiotic resistance of bacterial biofilms." International Journal of Antimicrobial Agents **35**(4): 322-332.

18. Darouiche, R. O., et al. (1994). "Vancomycin penetration into biofilm covering infected prostheses and effect on bacteria." Journal of Infectious Diseases **170**(3): 720-723.

19. Olsen, I. (2015). "Biofilm-specific antibiotic tolerance and resistance." European Journal of Clinical Microbiology & Infectious Diseases **34**(5): 877-886.

20. Ito, A., et al. (2009). "Increased Antibiotic Resistance of Escherichia coli in Mature Biofilms." Applied and Environmental Microbiology **75**(12): 4093-4100.

21. Antunes, A., et al. (2011). "High vancomycin resistance among biofilms produced by Staphylococcus species isolated from central venous catheters." Memorias Do Instituto Oswaldo Cruz **106**(1): 51-55.

22. Claessens, J., et al. (2015). "Inefficacy of vancomycin and teicoplanin in eradicating and killing Staphylococcus epidermidis biofilms in vitro." International Journal of Antimicrobial Agents **45**(4): 368-375.

23. Sakimura, T., et al. (2015). "Biofilm-Forming Staphylococcus epidermidis Expressing Vancomycin Resistance Early after Adhesion to a Metal Surface." Biomed Research International: 8.

24. Takahashi, H., et al. (2009). "Antimicrobial prophylaxis for spinal surgery." Journal of Orthopaedic Science **14**(1): 40-44.

25. O'Neill, K. R., et al. (2011). "Reduced surgical site infections in patients undergoing posterior spinal stabilization of traumatic injuries using vancomycin powder." The Spine Journal **11**(7): 641-646.

26. Molinari, R. W., et al. (2012). "Prophylactic intraoperative powdered vancomycin and postoperative deep spinal wound infection: 1,512 consecutive surgical cases over a 6-year period." European Spine Journal **21**(S4): 476-482.

27. Argenta, L. C. and M. J. Morykwas (1997). "Vacuum-assisted closure: A new method for wound control and treatment: Clinical experience." Annals of Plastic Surgery **38**(6): 563-576.

28. Morykwas, M. J., et al. (1997). "Vacuum-assisted closure: A new method for wound control and treatment: Animal studies and basic foundation." Annals of Plastic Surgery **38**(6): 553-562.

29. Hetrick, E. M. and Schoenfisch, M. H. (2006). "Reducing implant-related infections: active release strategies." Chemical Society Reviews **35**(9): 780-789.

30. Mei, L., et al. (2014). "Antimicrobial activity of Ag surfaces sputtered by magnetron sputtering." Materials Research Innovations**18**: 875-878.

31. Lambadi, P. R., et al. (2015). "Facile biofunctionalization of silver nanoparticles for enhanced antibacterial properties, endotoxin removal, and biofilm control." International Journal Nanomedicine **10**: 2155-2171.

32. Sin, M. C., et al. (2014). "Zwitterionic-Based Stainless Steel with Well-Defined Polysulfobetaine Brushes for General Bioadhesive Control." ACS Applied Materials & Interfaces **6**(2): 861-873.

33. Michl, T. D., et al. (2015). "Nitric oxide releasing plasma polymer coating with bacteriostatic properties and no cytotoxic side effects." Chemical Communications **51**(32): 7058-7060.

34. Williams, D. L., et al. (2014). "In Vitro Efficacy of a Novel Active-Release Antimicrobial Coating To Eradicate Biofilms of Pseudomonas aeruginosa." Antimicrobial Agents and Chemotherapy **58**(4): 2400-2404.

35. Xiao, D. Q., et al. (2014). "Room-temperature attachment of PLGA microspheres to titanium surfaces for implant-based drug release." Applied Surface Science **309**: 112-118.

36. He, N. A., et al. (2011). "Enhancement of Vancomycin Activity against Biofilms by Using Ultrasound-Targeted Microbubble Destruction." Antimicrobial Agents and Chemotherapy **55**(11): 5331-5337.

37. Dong, Y., et al. (2013). "Synergy of ultrasound microbubbles and vancomycin against Staphylococcus epidermidis biofilm." Journal of Antimicrobial Chemotherapy **68**(4): 816-826.

38. Lin, T., et al. (2015). "In Vitro and In Vivo Evaluation of Vancomycin-Loaded PMMA Cement in Combination with Ultrasound and Microbubbles Mediated Ultrasound." Biomed Research International: 7.

39. Loike, J. D., et al. (2013). "Surface Acoustic Waves Enhance Neutrophil Killing of Bacteria." PloS One **8**(8): 7.

40. Mavrogenis, A. F., et al. (2014). "PEEK rod systems for the spine." European Journal of Orthopaedic Surgery & Traumatology **24**(S1): 111-116.

41. Ni, J., et al. (2015). "Radiological evaluation of anterior lumbar fusion using PEEK cages with adjacent vertebral autograft in spinal deformity long fusion surgeries." European Spine Journal **24**(4): 791-799.

42. Kurtz, S. M. (2012). "PEEK Biomaterials Handbook." Pp: 2-4.

43. Kurtz, S. M. and J. N. Devine (2007). "PEEK biomaterials in trauma, orthopedic, and spinal implants." Biomaterials **28**(32): 4845-4869.

44. El Halabi, F., et al. (2011). "Mechanical characterization and numerical simulation of polyether–ether–ketone (PEEK) cranial implants." Journal of the Mechanical Behavior of Biomedical Materials **4**(8): 1819-1832.

45. Kruth, J. P., et al. (2003). "Lasers and materials in selective laser sintering." Assembly Automation **23**(4): 357-371.

46. S. Beretta, O. G., K. E. Evans, A. Anderson, C. Newman (2013). "Size, shape and flow of powders for use in Selective Laser Sintering (SLS)." Proceedings of VRAP 2013 6th International Conference on Advanced Research in Virtual and Rapid Prototyping: pp. 49 - 54.

47. Schmidt, M., et al. (2007). "Selective Laser Sintering of PEEK." CIRP Annals – Manufacturing Technology **56**(1): 205-208.

48. Friedman, S. P. and N. A. Seaton (1995). "A corrected tortuosity factor for the network calculation of diffusion coefficients." Chemical Engineering Science **50**(5): 897-900.

49. Pismen, L. M. (1974). "Diffusion in porous media of a random structure." Chemical Engineering Science **29**(5): 1227-1236.

50. Baughman, G. L., et al. "Dye Solubilities. In: Advances in Color Chemistry." Freeman M, Peters MT, eds., Elsevier (1993).

51. Leaist, D. G. (1988). "The effects of aggregation, counterion binding, and added NaCl on diffusion of aqueous methylene blue." Canadian Journal of Chemistry **66**(9): 2452-2457.

52. Sarkar, D. (2010). "Adsorptive Mass Transport of Dye on Rice Husk Ash." Journal of Water Resource and Protection **2**(5): 424-431.

53. Vadivelan, V. and K. V. Kumar (2005). "Equilibrium, kinetics, mechanism, and process design for the sorption of methylene blue onto rice husk." Journal of Colloid and Interface Science **286**(1): 90-100.

54. Shen, L. and Z. Chen (2007). "Critical review of the impact of tortuosity on diffusion." Chemical Engineering Science **62**(14): 3748-3755.

55. Tomadakis, M. M. and S. V. Sotirchos (1993). "Transport properties of random arrays of freely overlapping cylinders with various orientation distributions." The Journal of Chemical Physics **98**(1): 616-626.

56. Wrenn, S. P., et al. (2012). "Bursting bubbles and bilayers." Theranostics **2**(12): 1140-1159.

57. Deckers, R. and C. T. W. Moonen (2010). "Ultrasound triggered, image guided, local drug delivery." Journal of Controlled Release **148**(1): 25-33.

58. Pua, E. C. and Z. Pei Zhong Pei (2009). "Ultrasound-mediated drug delivery." IEEE Engineering in Medicine and Biology Magazine **28**(1): 64.

59. Yan, F., et al. (2012). "Paclitaxel-liposome loaded microbubbles for ultrasound triggered drug delivery in vitro and in vivo." The Journal of the Acoustical Society of America **131**(4): 3366-3366.

60. Lammertink, B., et al. (2015). "Duration of ultrasound-mediated enhanced plasma membrane permeability." International Journal of Pharmaceutics **482**(1 2): 92-98.

61. Sjollema, J., et al. (2014). "On-demand antimicrobial release from a temperature sensitive polymer - Comparison with ad libitum release from central venous catheters." Journal of Controlled Release **188**: 61-66.

62. Borges, J., et al. (2014). "Layer-by-Layer Assembly of Light-Responsive Polymeric Multilayer Systems." Advanced Functional Materials **24**(36): 5624-5648.

63. ter Boo, G. J. A., et al. (2015). "Antimicrobial delivery systems for local infection prophylaxis in orthopedic- and trauma surgery." Biomaterials **52**: 113-125.

64. Zhuk, I., et al. (2014). "Self-Defensive Layer-by-Layer Films with Bacteria-Triggered Antibiotic Release." Acs Nano **8**(8): 7733-7745.

65. Ulery, B. D., et al. (2011). "Biomedical applications of biodegradable polymers." Journal of Polymer Science Part B: Polymer Physics **49**(12): 832-864.

66. Wang, H., et al. (2008). "Hollow porous poly(lactic acid) microspheres." Journal of Applied Polymer Science **107**(2): 1189-1193.

67. Park, T. G. (1995). "Degradation of poly(lactic-co-glycolic acid) microspheres: effect of copolymer composition." Biomaterials **16**(15): 1123-1130.

68. Anderson, J. M. and M. S. Shive (2012). "Biodegradation and biocompatibility of PLA and PLGA microspheres." Advanced Drug Delivery Reviews **64, Supplement**(0): 72-82.

69. Lindsey, C., et al. (2006). "The effects of rod contouring on spinal construct fatigue strength." Spine **31**(15): 1680-1687.

70. Baxter, R. M., et al. (2013). "Characteristics of highly cross-linked polyethylene wear debris in vivo." Journal of Biomedical Materials Research. Part B, Applied Biomaterials **101**(3): 467-475.